

1 **Relative sea-level data from southwest Scotland constrain meltwater-driven sea-level**  
2 **jumps prior to the 8.2 kyr BP event**

3 Thomas Lawrence\*<sup>1</sup>, Antony J. Long<sup>1</sup>, W. Roland Gehrels<sup>2</sup>, Luke Jackson<sup>3</sup>, David E. Smith<sup>4</sup>

4

5 <sup>1</sup>Dept. of Geography, Lower Mountjoy, Durham University, South Road, Durham, DH1 3LE

6 <sup>2</sup>Environment Dept., York University, Heslington, York, YO10 5NG

7 <sup>3</sup>New Institute for Economic Thinking, Eagle House, Oxford University, OX2 6ED

8 <sup>4</sup>Geography and Environment Dept., St Edmund Hall, Oxford University, OX1 4AR

9

10 \*corresponding author (thomas.lawrence@durham.ac.uk)

11 Keywords: sea level, 8.2 ka event, early Holocene, ice-sheet, lake drainage, Scotland

12

13 **Abstract**

14 The most significant climate cooling of the Holocene is centred on 8.2 kyr BP (the ‘8.2  
15 event’). Its cause is widely attributed to an abrupt slowdown of the Atlantic Meridional  
16 Overturning Circulation (AMOC) associated with the sudden drainage of Laurentide  
17 proglacial Lakes Agassiz and Ojibway, but model simulations have difficulty reproducing the  
18 event with a single-pulse scenario of freshwater input. Several lines of evidence point to  
19 multiple episodes of freshwater release from the decaying Laurentide Ice Sheet (LIS)  
20 between ~8900 and ~8200 cal yr BP, yet the precise number, timing and magnitude of these  
21 events – critical constraints for AMOC simulations – are far from resolved. Here we present a  
22 high-resolution relative sea level (RSL) record for the period 8800 to 7800 cal yr BP  
23 developed from estuarine and salt-marsh deposits in SW Scotland. We find that RSL rose  
24 abruptly in three steps by 0.35 m, 0.7 m and 0.4 m ( $\mu$ ) at 8760-8640, 8595-8465, 8218-8323  
25 cal yr BP respectively. The timing of these RSL steps correlate closely with a variety of  
26 short-lived events expressed in North Atlantic proxy climate and oceanographic records,  
27 providing evidence of at least three distinct episodes of enhanced meltwater discharge from  
28 the decaying LIS prior to the 8.2 event. Our observations can be used to test the fidelity of  
29 both climate and ice-sheet models in simulating abrupt change during the early Holocene.

30

31

## 32 1. Introduction

33

34 A prominent climate anomaly is centred on 8200 yr BP in Greenland ice-core records (Figs. 1  
35 and 2) and is registered as an abrupt cooling of  $\sim 3.3 \pm 1.1$  °C that lasted for 160 yrs (Kobashi  
36 et al., 2007; Thomas et al., 2007). The widely cited (e.g. Alley et al., 1997; De Vernal et al.,  
37 1997; Barber et al., 1999; Törnqvist and Hijma, 2012) causal mechanism of the event is a  
38 weakening or complete shutdown of the Atlantic Meridional Overturning Circulation  
39 (AMOC) in response to the sudden drainage of Laurentide proglacial Lakes Agassiz and  
40 Ojibway (LAO) dated to 8740-8160 cal yr BP ( $1\sigma$  age range) in the Hudson region (Barber et  
41 al., 1999). However, it is unclear whether the drainage occurred as a standalone freshwater  
42 pulse or as several separate events. Indeed, climate modelling studies based on a single  
43 freshwater pulse of 2.5 Sv for one year (Sverdrup,  $1.0 = 10^6 \text{ m}^3 \text{ s}^{-1}$ ) fail to simulate the  
44 observed 8.2 climatic response (Morrill et al., 2014) using a median estimate of forcing  
45 inferred from flood hydrograph simulations of the final LAO drainage (Clarke et al., 2004).

46 A growing body of empirical and modelling evidence is beginning to support a multi-  
47 event model of LAO drainage (Leverington et al., 2002) and/or nonlinear Laurentide Ice  
48 Sheet (LIS) collapse within a critical time interval (hereby referred to as 8900 to 8200 cal yr  
49 BP). Pronounced two-step increases in planktonic  $\delta^{18}\text{O}$  and polar foraminifera abundance  
50 (*Neogloboquadrina pachyderma* s.) occur in two sub-polar North Atlantic cores, MD99-2251  
51 and MD03-2665, situated 1250 km apart, that are interpreted as two episodes of increased  
52 surface ocean freshening and cooling within this time interval (Fig. 2; Ellison et al., 2006;  
53 Kleiven et al., 2008). Hematite-rich glaciolacustrine sediments in the Hudson region (the  
54 “red-bed”) widely thought to represent the stratigraphic signature of LAO drainage (e.g.  
55 Barber et al., 1999; Hillaire-Marcel et al., 2007), contain two peaks of terrestrially-sourced  
56 detrital carbonate (Hillaire-Marcel et al., 2007) and two stacked sequences of reverse to  
57 normal graded sediments which could record two separate drainage events (Lajeunesse and  
58 St-Onge, 2008).

59 Recent evidence from shelf-sea and estuarine sediments complicate the story as these  
60 contain evidence of a third event. A well-resolved near-field record of LIS retreat is provided  
61 by Jennings et al. (2015), who observed detrital carbonate peaks (DCPs) at 8694-8609  
62 (DCP6a), 8609-8489 (DCP6b) and 8219-7998 cal yr BP (DCP7) (Fig. 2g) in Cartwright  
63 Saddle core MD99-2236, which they attribute to episodes of abrupt freshwater discharge. The  
64 second event, DCP6b, is manifest as the downstream equivalent of the Hudson Bay “red-

65 bed”, which Jennings et al. (2015) re-interpret as a final phase in the abrupt opening of the  
66 Tyrrell Sea following retreat of Laurentide ice – not a drainage of LAO. Recent ice-sheet  
67 modelling predicts that the dynamic separation, or “saddle-collapse” of the Keewatin and  
68 Labrador domes, which occurred during deglaciation over the Tyrrell Sea, produced a  
69 meltwater pulse with peak discharge rates of ~0.21 Sv between ~8800 and ~8600 yrs BP  
70 (Gregoire et al., 2012). This provides a possible mechanism for a meltwater pulse  
71 concomitant with the Tyrrell Sea ‘opening’ event. Jennings et al. (2015) interpret the later  
72 event, DCP7, as the signature of LAO drainage(s) due to its close coincidence with the 8.2  
73 event. However the significance of DCP7 in forcing the 8.2 event is unclear as it post-dates  
74 the onset of the 8.2 event, dated at ~8247 cal yr BP (Thomas et al., 2007), by a minimum c.  
75 30 yrs, albeit this could reflect chronological uncertainties within the Jennings et al. (2015)  
76 record (i.e., the 8.2 to 9.7 ka BP time interval is constrained in this record by two <sup>14</sup>C ages).  
77 Nevertheless, this three-event model of abrupt freshwater discharge is supported by estuarine  
78 records from the Gulf of Mexico where Simkins et al. (2012) observed prominent magnetic  
79 susceptibility anomalies at ~8800, ~8600 and ~8100 cal yr BP. It is suggested that previous  
80 near-field sea-bed records that describe evidence of one or two events (Hillaire-Marcel et al.,  
81 2007; Hoffman et al., 2012) are limited by core resolution and may record additional events  
82 (Jennings et al., 2015).

83 Notwithstanding the limited chronological control across the critical time interval, the  
84 Cartwright Saddle record from core MD99-2236 arguably provides the best-resolved near-  
85 field history of final LIS retreat because of its relatively high resolution and stratigraphic  
86 continuity. The interpretation of a three-event freshwater discharge model includes the  
87 potential abrupt drainage(s) of LAO as well as a possible large ice-sheet contribution  
88 associated with the saddle collapse of the Keewatin and Labrador domes (Gregoire et al.,  
89 2012). If correct, the causal mechanisms of the 8.2 event are more complex than that  
90 suggested by the consensus view of a single- or double-event drainage of LAO. The Jennings  
91 et al. (2015) record describes a sequence of freshwater events prior to the 8.2 event but little  
92 is known regarding the magnitudes of such events, critical constraints for modelling studies  
93 of the AMOC. Understanding the pathways of freshwater routing is also critical as some  
94 authors predict transport into the sub-tropical North Atlantic (Condrón and Windsor, 2011;  
95 Hill and Condrón, 2014) rather than the sub-polar gyre (Jennings et al., 2015; Kleiven et al.,  
96 2008; Ellison et al., 2006).

97 Relative sea-level (RSL) records provide a means to test the hypothesis that the DCP  
98 events in Cartwright Saddle core MD99-2236 were significant freshwater discharge events  
99 from the LIS. Regional land-based water/ice mass variability will alter the geoid thus  
100 producing an associated sea-level pattern, also termed “fingerprint”, that is non-uniform  
101 across the globe (e.g. Mitrovica et al., 2001). In the case of a point source of land water/ice  
102 mass loss, RSL will be negative near to the former source location and positive in the  
103 intermediate to far-field regions. This is illustrated in Fig. 1, which shows the predicted  
104 percentage of the global sea-level equivalent mass loss from the drainage of Lake Agassiz-  
105 Ojibwa at 8.4ka (Kendall et al., 2008) using a geophysical model to solve the sea-level  
106 equation (Mitrovica & Milne, 2003).

107 Three well-dated RSL records based on radiocarbon-dated basal peats (therefore  
108 minimally affected by sediment compaction) exist for the centuries prior 8.2 ka, and both  
109 contain an abrupt departure from background rates of RSL rise, or a RSL ‘jump’. In the  
110 western Netherlands (Rhine-Meuse Delta), Hijma and Cohen (2010) define a eustatic  
111 equivalent sea-level jump of  $3.0 \pm 1.5$  m at 8590-8350 cal yr BP, while in the Mississippi  
112 Delta, Li et al. (2012) identify a eustatic jump of  $1.2 \pm 0.2$  m at 8310-8180 cal yr BP. Both  
113 jumps are corrected for a Laurentide source of mass loss using geophysical modelling  
114 predictions (Kendall et al., 2008). It has been suggested that due to differences in the timing  
115 and magnitude of the two RSL jumps, the Rhine-Meuse jump contains two separate events,  
116 while the Mississippi Delta record captures a final event only (Törnqvist and Hijma, 2012; Li  
117 et al., 2012). Indeed, the Mississippi Delta record contains a reworked pre-event stratigraphy  
118 dated to ~8400 cal yr BP which has been interpreted as possible evidence of a preceding RSL  
119 jump (Li et al., 2012). The third well-dated RSL record is from the Ythan estuary, Scotland,  
120 and discloses a RSL jump of between 2.56m and 4.77m, dated at between 8177-8366 cal yr  
121 BP and 8445-8637 cal yr BP ( $2\sigma$  ranges), but no evidence for more than one jump is quoted  
122 (Smith et al., 2013).

123 The Rhine-Meuse, Mississippi Delta and Ythan estuary records lack conclusive bio-  
124 and lithostratigraphic evidence of more than one event found in continuous stratigraphic  
125 sequence. Therefore, at present the sea-level data are unable to test the hypothesised three-  
126 stage LIS retreat model of Jennings et al. (2015).

127 Here we present a stratigraphically continuous record of RSL for Blair’s Croft in the  
128 Cree Estuary, SW Scotland, which is sub-centennially resolved for the period ~8800 to ~7800  
129 cal yr BP. In particular, we test two hypotheses: (1) that RSL rose abruptly in more than one

130 abrupt step in the several centuries prior to 8.2 event, and (2) that the RSL jump(s) correlate  
131 with other short-lived event(s) observed in various North Atlantic proxy records.

132

## 133 **2. Field site**

134

135 The Cree Estuary is situated on the northern shores of the Solway Firth (N 54°51', W 4°30').  
136 The River Cree is tidal from Newton Stewart and drains southwards through the Cree coastal  
137 lowlands into Wigtown Bay (Fig. 3B). The predicted present day spring tidal range in  
138 Wigtown Bay is 6.40 m (supplementary info Fig. S1; Ward, 2014), which is comparable to  
139 the range of 6.70 m obtained from the tide gauge in the adjacent small (up-) estuary harbour  
140 of Kirkcudbright (Fig. 3B; Admiralty Tide Tables, 2014). The Cree coastal lowlands (i.e., the  
141 area below the 10 m OD (OD = UK geodetic datum; where 0 m OD = approximate mean tide  
142 level) contour line; Fig. 3C) have been the focus of several previous RSL studies (e.g.  
143 Jardine, 1975; Bishop and Coope, 1977; Smith et al., 2003a). In the most recent of these,  
144 Smith et al. (2003a) reported that RSL rose from -6 m OD at ~9500 to a mid-Holocene RSL  
145 highstand of +6 m OD at ~5500 cal yr BP before falling to present. One of the sites used to  
146 constrain this RSL history is Blair's Croft, located ~1.5 km inland of the current tidal limit  
147 and at the base of the Galloway National Park foothills, where a sequence of interbedded  
148 estuarine and salt-marsh deposits are preserved below a surface freshwater peat. These  
149 deposits were dated by Smith et al. (2003a) using conventional bulk radiocarbon dating to  
150 within the broad timeframe of the 8.2 event, although not fully attributed to the event itself.  
151 These sediments provide the basis for this study.

152

## 153 **3. Methods**

### 154 **3.1 Lithostratigraphy**

155

156 We conducted further lithostratigraphic investigations at Blair's Croft, paying particular  
157 attention to the sediments that were originally dated by Smith et al. (2003a) as spanning the  
158 centuries either side of the 8.2 event, i.e. between ~8800 and 7800 cal yr BP (Figs. 4 and 5).  
159 Fifty hand-cores were sunk along three transects. Sediments were classified with reference to

160 the Troels-Smith (1955) scheme of stratigraphic notation. Each transect commenced at the  
161 break of slope at the valley-side and extended westward by 100-200 m towards the A75 trunk  
162 road and the present-day estuary. No further cores were sunk on the western side of the A75  
163 road in Carsewolloch Flow, as Smith et al. (2003a) and Wells (1997) here reported a broadly  
164 homogenous sequence of estuarine clays (i.e., no inter-bedded organic deposits). Sample core  
165 BC421 (Transect 1) was deemed representative of wider changes at Blair's Croft and was  
166 collected using a modified piston corer with 0.7-1.0 m overlapping lengths. Some compaction  
167 was observed during sampling and corrected for based on the depths recorded in an adjacent  
168 hand core. We account for this correction with a conservative 0.2 m uncertainty (Section 3.4).

169

### 170 **3.2 Laboratory methods**

171

172 We conducted microfossil (diatom) analyses in order to determine estimates of past sea level.  
173 Samples were prepared using standard techniques (Palmer and Abbott, 1986), identified with  
174 reference to the taxonomy of Hartley et al. (1996) and grouped according to a simplified  
175 halobian classification scheme of Vos and de Wolf (1993). A total of 74 samples were taken  
176 at ~4 cm intervals. We counted a minimum of 200 valves, with the exception of 10 samples  
177 that contained a count of 150-200 valves. Percentage loss-on-ignition was measured on 4 g  
178 subsamples to identify horizons with relatively high organic content (>20%) indicative of  
179 upper intertidal and supratidal conditions. Samples were weighed prior to being oven-dried  
180 overnight at 80°C, reweighed, combusted at 550°C for four hours and weighed again.

181 Our chronology is constrained by 13 Accelerator Mass Spectrometry (AMS) <sup>14</sup>C  
182 determinations of individual terrestrial plant macrofossils (Table 1). Ages are reported as 2σ  
183 ranges, calibrated (IntCal13; Reimer et al., 2013) with respect to BP (where BP = AD 1950).  
184 Our dating was performed at the Scottish Universities Environmental Research Centre,  
185 NERC radiocarbon facility in East Kilbride, UK, on cleaned, horizontally-bedded plant  
186 macrofossils (*Phragmites australis*) and c. 1cm<sup>3</sup> wood (*Alnus*) fragments that were intact and  
187 away from the core edges. All <sup>14</sup>C samples were pre-treated using standard methods (e.g.  
188 Czernik and Goslar, 2001) in East Kilbride. Most samples were dated twice and subject to a  
189 weighted mean using the "R\_combine" function of OxCal 4.2 (Bronk Ramsey, 2008) in an  
190 attempt to increase the precision of uncalibrated <sup>14</sup>C ages (i.e. the reported 1σ laboratory  
191 errors, Marshall et al., 2007; Li et al., 2012). Ages were modelled with an OxCal 4.2  
192 "P\_Sequence" function, which takes into account stratigraphic information and thus assumes

193 that calibrated ages increase with depth, i.e., that no age reversals are allowed. Such models  
194 have shown to improve accuracy and retain precision (e.g. Bronk Ramsey, 2000).

195

### 196 3.3 Transfer function development

197

198 To reconstruct RSL from fossil diatom assemblages, we exploit the relationship between the  
199 distribution of their modern counterparts with marsh surface elevation (e.g. Zong and Horton,  
200 1999; Barlow et al., 2013), which is primarily controlled by the frequency of tidal flooding  
201 (hence, RSL). The elevation of an assemblage relative to tide levels is termed its ‘indicative  
202 meaning’. Underpinning this is the assumption that the indicative meanings of contemporary  
203 diatoms and their assemblages remain unchanged through time. We apply the Barlow et al.  
204 (2013) transfer function to our fossil assemblages using the computer software C<sup>2</sup> v.1.6  
205 (Juggins, 2011). The Barlow et al. (2013) dataset, although based on nine separate modern  
206 records from western Scotland, is lacking a key taxon that forms a large component of the  
207 Blair’s Croft fossil record, *Tryblionella navicularis*, and which is essential to our  
208 reconstruction. Within present-day UK salt-marshes this taxon has only been documented in  
209 suitable abundances in Brancaster Marsh, Norfolk, eastern England, where it is found around  
210 the level of MHWST within an area characterised by *Phragmites australis* (supplementary  
211 info Fig. S2; Gehrels et al., 2001). In view of the abundance of *P. australis* macrofossil  
212 remains in the Blair’s Croft organic beds, these appear to be analogous environments. All  
213 taxa from the Brancaster samples are included in addition to *T. navicularis*, which are  
214 integrated by standardizing their elevations (with respect to tidal range) with the standard  
215 water level index (SWLI) equation (Barlow et al., 2013):

216

$$217 \text{SWLI}_n = 100(h_n - h_{\text{MTL}}) / (h_{\text{MHWST}} - h_{\text{MTL}}) + 100 \quad (1)$$

218

219 where  $\text{SWLI}_n$  is the standard water level index for a given sample  $n$ ,  $h_n$  is the elevation of a  
220 given sample  $n$  (in metres OD),  $h_{\text{MHWST}}$  is the local mean height of spring tide and  $h_{\text{MTL}}$  is the  
221 local height of mean tide level. A SWLI of 100 and 200 are equivalent to MTL and MHWST,  
222 respectively.

223           Transfer function-based estimates of palaeo-RSL are calculated with respect to the  
224 modern tidal regime so they require correction for palaeotidal change. Estimates of the  
225 elevation of the height of MHWST for Wigtown Bay are provided by the palaeotidal model  
226 of Ward (2014), which indicates a reduction in MHWST height (based on  $M_2 + S_2$  tidal  
227 components) from 3.27 m OD at 9.0 ka BP to 3.00 m OD at 8.0 ka BP (supplementary info  
228 Fig. S1). As most of our record encompasses this 1 kyr interval, we correct our data points  
229 using simple linear interpolation of the points between the 9.0 and 8.0 ka BP time-slices  
230 (supplementary info Fig. S1). We assume a fixed height of MTL (=0 m OD) across the time  
231 interval, such that the only fluctuating variable is MHWST height. The resulting correction  
232 applied is specific to each data point and uses the corresponding age inferred from the age  
233 model. No attempt was made to correct the few samples younger than 8.0 ka BP with a  
234 second linear function for the 8.0 to 7.0 ka BP time period; instead we extrapolate the same  
235 linear function. Uncertainties in the Ward (2014) model are yet to be rigorously quantified  
236 (Ward, pers. comm), so we introduce an arbitrary measure of uncertainty of 0.20 m for each  
237 data point. This is significantly larger than 2 standard error of the mean of the palaeotidal  
238 data (0.06 m) (Section 3.4). Transformation of the SWLI values back to OD is achieved  
239 using:

$$240$$
$$241 \quad OD_n = (SWLI_n - 100) \times (PTH_{MHWST} - PTH_{MTL}) / 100 \quad (2)$$

242

243 where  $OD_n$  is the height of a given sample relative to ordnance datum,  $SWLI_n$  is the standard  
244 water level index of a given sample,  $PTH_{MHWST}$  is the local height of mean high water of  
245 spring (palaeo)tide for the appropriate time period of interest (inferred from the age model)  
246 and  $PTH_{MTL}$  is the local height of mean (palaeo) tide level for the appropriate time period of  
247 interest (assumed zero).

248

### 249   **3.4   Sea-level reconstruction**

250

251 The combined uncertainty of each RSL data point comprises three error components  
252 (supplementary info Table S1); a) bootstrapped 1 SEM values of indicative meanings  
253 predicted by the modified Barlow et al. (2013) transfer function that includes *T. navicularis*  
254 (average +0.56 m;  $1\sigma$ ) and, b) the uncertainty of the palaeotidal correction (0.20 m). Thirdly,



255 we have linearly corrected for the difference between logged depths in a hand core and  
256 extruded depths from a piston core, for which we conservatively introduce a further 0.20 m to  
257 account for. All of the above terms are expressed as bidirectional  $1\sigma$  uncertainties. We  
258 propagate these individual terms in a mean squared estimate to produce a combined  
259 uncertainty for each data-point:

$$260 \text{ Mean squared estimate} = \sqrt{a^2 + b^2 + c^2} \quad (3)$$

261 The indicative meanings for each data point are converted to RSL using:  $S = H - I$ ,  
262 where  $S$  is the height of relative sea-level (m OD),  $H$  is the height of the given sample (m  
263 OD) and  $I$  is the indicative meaning of the fossil sample (m OD).

264 To perform the sea-level reconstruction, we adapt the method of Rohling et al. (2014)  
265 by altering our method of random sampling in time and space. The conservative approach to  
266 constructing random samples from a set of RSL indicators is to randomly sample each in time  
267 independently and space independently. This approach assumes the RSL indicators are  
268 independent in terms of their relationship to each other. Problematically an individual RSL  
269 realisation (one sample drawn from each indicator), from the independently sampled data set  
270 may have reversals in time and space due to the overlapping uncertainties of adjacent  
271 indicators. In the case where data is derived from a single core, with stratigraphic order to  
272 the indicators, the conservative sampling method is physically implausible. To account for  
273 this dependency, yet allow for each RSL indicator to remain randomly sampled, we use the  
274 following strategy. We randomly sample the first and second RSL indicators. For each  
275 sample of the first RSL indicator we identify which quantile it falls within in time and space.  
276 We then tie it to a sample from the second RSL indicator drawn from those lying in the same  
277 time/space quantiles as the first. The next RSL indicator is then randomly sampled and each  
278 sample in the previous indicator tied to one in the newly sampled indicator. By applying this  
279 method to the set of RSL indicators we retain their order whilst sampling each randomly. We  
280 produce 1000 realisations of the RSL indicators, sampling each RSL indicator 1000 times.  
281 This novel approach to sampling is an attempt to reduce the uncertainties of the  
282 reconstruction given the wide uncertainties in time and space of the RSL indicators relative to  
283 the decimetre and decadal-to-centennial scale of DCP events that we seek to identify.

284 The remaining part of the reconstruction method follows Rohling et al. (2014), where  
285 we linearly interpolate each of the 1000 realisations to create time series with 10 year step  
286 size. We then calculate mean and standard deviations of the interpolated realisations at each

287 time step. We also remove spurious fluctuations by smoothing the reconstructed curves with  
288 a 50 year moving window. This degree of smoothing is minimal and does not significantly  
289 influence the results.

290 To determine rates of RSL, we employ two methods. The first is a sea-level rate  
291 reconstruction that uses the same method as outlined above, but differentiates a smoothed  
292 version of each linearly interpolated realisation. Following this, we calculate mean and  
293 standard deviations of the derived rates at each time step. The second approach is to  
294 differentiate the smoothed RSL reconstruction and its uncertainty bounds. While the first  
295 method is conservative in that it represents the full range of uncertainty in the rate derived  
296 from random sampling, the second assumes that the shape of RSL reconstruction is true,  
297 regardless of its vertical offset from the mean. For each method, the mean RSL rate  
298 reconstruction ( $\mu_{dRSL/dt}$ ) and differentiated mean RSL reconstruction ( $d\mu_{RSL/dt}$ ) give  
299 effectively the same result (see Results).

300

### 301 **3.5 Developing comparative chronologies from ocean and ice core records**

302

303 We test hypothesis (2); whether the timing of RSL jumps correlate with other abrupt events  
304 expressed in North Atlantic proxy records, by comparing the timing of sea-level  
305 accelerations/jumps within our record with those observed in various climate proxy records  
306 from the North Atlantic. Where resolution permits, we focus on comparing the start of events  
307 rather than event maxima within their respective chronologies.

308

#### 309 **3.5.1 Inferring the timing of abrupt North Atlantic events**

310 We infer the onset of the two-step increases recorded in the surface  $\delta^{18}\text{O}$  record from the  
311 North Atlantic (FE<sub>1</sub> and FE<sub>2</sub>; Fig. 2h) (Kleiven et al., 2008) following new age modelling of  
312 the Kleiven et al. (2008) chronology, which was previously based on simple linear  
313 interpolation of <sup>14</sup>C ages. The Kleiven et al. (2008) observations are supported by a second  
314 planktonic foraminiferal dataset retrieved some 1250 km away in core MD99-2251 which  
315 also contains two abrupt anomalies (Figs. 2e and 2h) (Ellison et al., 2006), although the  
316 records are offset by c. 250 yrs, likely because of the limited age control of MD99-2251. For  
317 instance the chronology for MD99-2251 (Ellison et al., 2006) contains only two ages within

318 the critical time interval compared to the nine in MD03-2665 (Kleiven et al., 2008). As a  
319 result, we do not include the Ellison et al. (2006) record in our comparison, but nevertheless  
320 assume that the two-step anomalies in both records are expressions of the same events  
321 (Kleiven et al., 2008) and that the age offset reflects the limitations of the Ellison et al. (2006)  
322 chronology.

323 Of the nine dates between 9.0 to 8.0 kyr BP in the Kleiven et al. (2008) record, two  
324 are reversed. To correct this offset Kleiven et al. (2008) introduced a local reservoir value  
325 ( $\Delta R$ ) of 23 yrs to account for an enhanced East Greenland Current coincident with North  
326 Atlantic freshwater perturbation(s). We are unable to assess the reliability of this  
327 interpretation, but it is one we follow given the internal consistency of  $\Delta R$  corrected ages. To  
328 ensure chronological robustness, we model the original Kleiven et al. (2008)  $^{14}\text{C}$  data in  
329 OxCal 4.2 using a *P\_sequence* function, after conservatively doubling (arbitrarily) the local  
330  $\Delta R$  uncertainties applied to the two ages with reversals. We then propagate the original  
331 laboratory  $1\sigma$  errors of each  $^{14}\text{C}$  age in a mean squared estimate. The modelled ages of  
332 MD03-2665 demonstrate strong internal agreement (96% overall model agreement index).

333 Next we infer the timing of the start of the two *N. pachyderma*  $\delta^{18}\text{O}$  peaks from the  
334 adjusted chronology of Kleiven et al. (2008). However, we need to determine the precise  
335 onset of each anomaly within MD03-2665 with respect to core depth. The first abrupt  
336 increase in  $\delta^{18}\text{O}$  occurs at 332 cm, while the initial drop in  $\delta^{13}\text{C}$  in benthic foraminifera  
337 occurs at 346 cm in the same core (equivalent to  $\sim 70$  yrs within the chronology). As this is  
338 likely indicative of a transfer delay between ocean surface and bottom waters in registering  
339 the freshwater anomaly (Kleiven et al. 2008), the earliest manifestation of the underlying  
340 anomaly, i.e.; the start of the  $\delta^{13}\text{C}$  excursion, is therefore a more accurate representation of  
341 the start of the underlying freshwater event. This is supported by an increase in magnetic  
342 properties that is coeval with the onset of the  $\delta^{13}\text{C}$  excursion. To infer the onset of the second  
343 anomaly, we have no choice but to use the  $\delta^{18}\text{O}$  record because the  $\delta^{13}\text{C}$  series records a  
344 broad minimum spanning several centuries rather than two distinct events.

345 From proximal to the former LIS margin we also include the timing of three DCPs  
346 observed in core MD99-2236 (Jennings et al., 2015). Improving the Jennings et al. (2015)  
347 chronology with Bayesian modelling is not necessary given that the critical interval of this  
348 record is constrained by only two ages. To tie in existing RSL observations from elsewhere,  
349 we compare age probability density functions of the onset of the Rhine-Meuse Delta RSL  
350 jump (Hijma and Cohen, 2010) and the full range of the Mississippi Delta RSL jump (Li et

351 al., 2012). Finally, although poorly constrained by dating, we also discuss the peak timing of  
352 the modelled Keewatin-Labrador ice-dome saddle collapse (Gregoire et al., 2012) and its  
353 possible significance within the sequence of observations. To provide insights into possible  
354 leads and lags, we calculate minimum and maximum age intervals between each event and  
355 the 8.2 event by subtracting the minimum and maximum estimates of their respective  $2\sigma$   
356 calibrated ranges (Table 2).

357

## 358 **4. Results**

### 359 **4.1 Lithostratigraphy**

360

361 Our lithostratigraphic survey confirms the complex sequence of minerogenic silts and  
362 laterally extensive beds of organic silt that were originally mapped by Smith et al. (2003a).  
363 The individual beds onlap the foot of the eastern hillside and can be traced ~100-200 m  
364 westward towards the present estuary (Fig. 4) where they mostly dip westward towards the  
365 estuary, indicating that the shallower, valley-side sediments are less compacted than those  
366 closer to the present estuary. Within the beds and often within overlying minerogenic  
367 deposits in small quantities we found macrofossil remains of *Phragmites australis*, a common  
368 indicator of a fringing salt-marsh environment (>MHWST) (e.g. Zong and Horton, 1999).  
369 The most prominent organic beds (traceable across at least two transects) are those that occur  
370 at ~3 m, ~5 m and ~7 m OD which we refer to as ‘lower’, ‘middle’ and ‘upper’ beds,  
371 respectively. They are dated in sample core BC421 (Transect 1) to ~8800, ~8200 and ~7800  
372 cal yr BP. The top of the lower and middle beds contain detrital, horizontally-bedded wood  
373 fragments that have been transported from the adjacent freshwater upland and are overlain by  
374 gray silty clays containing sparse well-humified flecks and minor layers (sub mm) of  
375 unidentified organic material. This is evidenced above the middle bed where LOI peaks and  
376 remains high across the transition to overlying minerogenic silt. These transitions from  
377 organic to minerogenic sedimentation may record evidence of marsh drowning. In contrast,  
378 the upper organic bed is overlain by freshwater peat and may record regression. Overall, LOI  
379 is high within the organic beds (20-60%) and low within the silts (5-10%; Fig. 6). The  
380 elevations of the upper and middle beds can be correlated laterally, although the lower  
381 organic bed is not present in the south of the site (Transect 3). There is also stratigraphic  
382 variability. For example, there is a locally constrained organic deposit in Transect 2 that rises

383 from ~7 m OD in the west to ~9 m OD at the valley-side. To provide a rigorous test of  
384 hypothesis (1), i.e.; whether RSL rose by more than one abrupt step prior to the 8.2 event, our  
385 focus is on the entire sedimentary sequence that embraces the lower and middle organic beds  
386 and their overlying minerogenic deposits within core BC421. Later, we discuss the potential  
387 regional-global sea-level significance of this depositional sequence.

388 In the south of Blair's Croft, a gravel barrier underlies the surface peat (Fig. 3). Wells  
389 (1997) traced this feature farther north towards the wooded part of Blair's Croft where it falls  
390 sharply in altitude and is overlain by minerogenic silts. In Transect 3, the upper organic bed  
391 at ~7 m OD is recorded on the landward and seaward sides of the barrier suggesting that it  
392 was in place at its present position after the deposition of the upper bed. Two ages from near  
393 the base of the upper bed (7917-7608 and 7923-7694 cal yr BP; Fig. 5) thus provide a  
394 maximum age of ~8000 cal yr BP of barrier formation, at least at its present position. The  
395 potential influence of a palaeo-barrier on the stratigraphy that pre-dates ~8000 cal yr BP is  
396 considered later in the discussion.

397

## 398 **4.2 Biostratigraphy**

399

400 In general, the organic beds are dominated by high frequencies of *Navicula peregrina*, a high  
401 marsh taxon (Fig. 6), while the minerogenic silts contain *T. navicularis*, *Nitzschia sigma*,  
402 *Diploneis smithii*, *Gyrosigma wansbeckii*, *Cocconeis scutellum* (all epipellic or epiphytic taxa)  
403 and *Paralia sulcata* (planktonic), which are indicative of lower intertidal saltmarsh/mudflat  
404 conditions. For brevity, epipellic and epiphytic taxa are hereafter collectively referred to as  
405 'benthic'.

406 The transition between the lower organic bed and the overlying silt is sharp (<2 mm),  
407 with the microfossils indicating an abrupt (but non-erosive) switch from high marsh to lower  
408 intertidal conditions (Fig. 6). The overlying minerogenic silt contains minor amounts of well-  
409 humified organics, including *in situ* roots alongside organic material washed onto the tidal  
410 flat from a higher elevation, indicating close proximity of a lower salt marsh environment. At  
411 ~530 cm the diatoms begin to record a gradual return to saltmarsh conditions, with *P. sulcata*  
412 giving way to increased frequencies of *T. navicularis*. Frequencies of *P. sulcata* undergo a  
413 second increase from 30% to 55% between 511 and 494 cm, above which benthic taxa are  
414 not present until 455 cm. This section of core is mostly barren, but two samples contain

415 thickly silicified planktonic taxa *Thalassiosira eccentrica*, *Podosira stillegera*, *Stephanopyxis*  
416 *turris* and *Rhaphoneis ampiceros*. Organic content is low (<3%) and the core log records an  
417 increase in clay content. Either side of this planktonic zone, relatively low frequencies of  
418 *Cocconeis scutellum* (<10%) indicate a mudflat setting. Overall these data indicate the abrupt  
419 drowning of an already low intertidal setting. Higher up in the overlying minerogenic silt  
420 between 451 and 414 cm, *D. smithii* and *N. sigma* indicate a gradual return to lower salt-  
421 marsh conditions and the establishment of the middle bed.

422         Accumulation of the middle bed between 414 and 389 cm and the presence of high  
423 frequencies of *N. peregrina* indicate a full establishment of high marsh conditions. The  
424 contact between the middle bed and overlying minerogenic sediment is sharp (<2 mm),  
425 although there are relatively gradual microfossil involving increased frequencies of *T.*  
426 *navicularis*, *P. sulcata* and *D. smithii*. A final return to full high-marsh conditions is indicated  
427 by renewed deposition of organic silt at 315 cm which forms the organic silt that underlies  
428 peat and contains high frequencies of *N. peregrina* throughout.

429         In summary, there are three stratigraphic levels that record intertidal drowning within  
430 the Blair's Croft stratigraphic record between 8.8 and 7.8 ka BP (Fig. S3). Summarised from  
431 bottom to top, these are: i) across the transition between the lower bed and its overlying  
432 minerogenic deposit (high marsh drowning), ii) within this overlying minerogenic deposit,  
433 across the full length of the 'planktonic zone' (low marsh/mudflat drowning), and, iii) across  
434 the transition between the middle bed and its overlying minerogenic deposit (high marsh  
435 drowning).

436

### 437 **4.3 Transfer function development**

438

439 We introduce new samples to the Barlow et al. (2013) transfer function to resolve the issue of  
440 a missing modern analogue (*T. navicularis*). The species environmental response of the data  
441 determines model selection choice; those with environmental gradients >2 standard deviation  
442 (SD) units are generally considered to respond unimodally and require a weighted averaging  
443 partial least squares (WA-PLS) regression model, while a simple weighted averaging (WA)  
444 model is appropriate for datasets with gradient lengths <2 SD (Birks, 1995). The original  
445 Barlow et al. (2013) dataset is strongly unimodal (4.08 SD units), which is retained after  
446 adding the additional samples from Brancaster Marsh. We therefore use WA-PLS regression

447 with bootstrapping (1000 permutations) cross validation (ter Braak and Juggins, 1993; Birks,  
448 1995) using the C<sup>2</sup> software v. 1.6 (Juggins, 2011). Fig. S6 and Table S2 (supplementary  
449 info) plots observed versus predicted and observed versus residuals of the full dataset, which  
450 now includes 27 samples from Brancaster Marsh (total = 231 samples).

451 To improve the predictive ability of the transfer function, the training set is ‘screened’  
452 of outlying samples. We follow Gehrels et al. (2005) who discount samples with residuals >1  
453 SD of SWLI, which removes 14 samples, leaving 217 samples. Fig. S6 and Table S3  
454 (supplementary info) illustrates the performance (observed versus predicted and observed  
455 versus residual plots) of the one-, two- and three-component models of the screened dataset.  
456 We select the WA-PLS model with two components over the one-component model on the  
457 basis of an improvement in  $r^2$  and RMSEP by >5% (after Barlow et al., 2013). Good  
458 agreement of the Brancaster Marsh samples is indicated by low residuals in the observed  
459 versus residual plot (supplementary info Fig. S6; red crosses). Detrended correspondence  
460 analysis (DCA) also indicates a good degree of similarity between most of the Brancaster  
461 Marsh samples with the pre-existing samples (supplementary info Fig. S7), giving us further  
462 confidence in the decision to integrate these samples.

463

#### 464 **4.4.1 Modern analogues**

465

466 Integration of the Brancaster Marsh data facilitates the inclusion of *T. navicularis* in the  
467 reconstruction but a further 27 taxa remain with no modern analogues (supplementary info  
468 Fig. S8). These are rare forms, however, so they have little impact on the reconstruction.

469 A more important issue, however, concerns the inclusion of *P. sulcata* in the  
470 reconstruction, a highly-siliceous planktonic taxon that is present in high abundance in the  
471 minerogenic silts and indeed mudflat settings elsewhere in the U.K. (Zong and Horton, 1999;  
472 Gehrels et al., 2001; Wilson and Lamb, 2011; Hill et al., 2007). Planktonic taxa are assumed  
473 to have an imprecise relationship with RSL because they can be allochthonous (i.e.,  
474 transported) although in the Cree fossil record, *P. sulcata* demonstrates gradual (linear)  
475 changes in abundance across the lithological transitions between organic mud and  
476 minerogenic mud. As its ecological optimum occurs around the elevation of the upper tidal  
477 flat in the modified Barlow et al. (2013) model, the ecological information on its distribution  
478 appears to be supported by stratigraphic changes. If not directly controlled by elevation, the

479 distribution of *P. sulcata* likely reflects other processes that are tightly coupled to elevation  
480 such as increased/decreased tidal influence. This presents a problem as we are unable to test  
481 the robustness of the ecological optimum of *P. sulcata* in the modified Barlow et al. (2013)  
482 model. However, we have no choice but to include it in the reconstruction as it provides  
483 constraints on the indicate meanings of tidal flat deposits and extends the vertical range of  
484 our reconstruction to these environments, which are critical to constraining a minimum  
485 magnitude of drowning events (i.e., abrupt transitions from organic to minerogenic  
486 sedimentation). In doing so we recognise that accurately interpreting genuine short-lived  
487 events within our reconstruction requires careful consideration of the assemblage  
488 contributions of *P. sulcata* and whether these are supported by lithostratigraphic and  
489 additional biostratigraphic information. This issue is further addressed in Section 5  
490 (Discussion).

491

#### 492 **4.4 Chronology**

493

494 The chronology is based on nine tie-points (a total of 13 AMS  $^{14}\text{C}$  ages, including a mixture  
495 of duplicate and single dates) that are modelled in stratigraphic sequence in OxCal v 4.2  
496 (Bronk Ramsey, 2009a) (Fig. S4). The model builds prior (unmodelled) probability  
497 distributions of  $^{14}\text{C}$  ages and compares them with posterior (modelled) densities using  
498 Bayesian analysis and Monte Carlo Markov Chain random sampling (Gilks et al., 2006). The  
499 agreement index provides a measure of overlap between the prior and posterior model  
500 densities, with agreement indices >60% the accepted threshold (Bronk Ramsey, 2008). In our  
501 model, there is good agreement between the prior and posterior densities; seven out of eight  
502 tie-points have an agreement index of >77%, while the one remaining tie-point has a  
503 satisfactory agreement of 61%. Posterior probability densities for each RSL (y) data-point  
504 were determined by inserting blank ages into the model at the relevant stratigraphic position  
505 using the Date() function. Finally, we introduce the assumption that organogenic and  
506 minerogenic sequences accumulate at different rates by introducing ‘boundaries’ at organic –  
507 minerogenic stratigraphic contacts as without their introduction we were unable to model the  
508 sequence with a satisfactory level of agreement.

509

510



## 511 4.5 Sea-level reconstruction

512

513 Prior to undertaking any probabilistic analysis of our fossil record we describe the  
514 reconstruction in its raw form. Fig. S10 plots transfer function output (SWLI) versus both  
515 depth (Fig. S10a) and modelled ages (Fig. S10b). The full dataset is presented in Table S1.  
516 We identify two sustained reductions in palaeo-marsh surface elevation that support our  
517 preliminary interpretations of marsh drowning based on biostratigraphy alone. The first  
518 (lowest) is between 627 cm (8791-8531) (all ages  $2\sigma$  with respect to cal yrs BP) and 610 cm  
519 (8850-8528) and corresponds stratigraphically with the transition between the lower organic  
520 bed and overlying minerogenic deposit. The second is found between 511 cm (8621-8381)  
521 and 445 cm (8497-8321) and reflects the minerogenic section of core dominated by  
522 planktonic taxa, which are under- and overlain by relatively high occurrences of benthic  
523 lower marsh taxa ('the planktonic zone') (Section 4.2). The upper section of the core contains  
524 a period of lower amplitude changes in SWLI albeit superimposed on a highly fluctuating  
525 record. Within this section we note the possible existence of a third event at the level that  
526 corresponds across the broad transition between the middle organic bed and overlying clay  
527 between 395 cm (8353-8229) and 360 cm (8227-8087) and registered as a sub-centennial  
528 scale period of lower amplitude SWLI oscillations.

529 Following transformation of the SWLI values to sea level we are now in a position to  
530 assess the evidence of marsh drowning probabilistically (Table S2). Fig. 7b shows the  
531 probabilistically determined RSL reconstruction in the Cree Estuary for the period 8800 to  
532 7800 cal yr BP. The reconstruction shows RSL rising around 3 mm/yr from 8800 to 8000 cal  
533 yr BP and a slowdown from 8000 to 7800 cal yr BP. The relatively wide  $1\sigma$  and  $2\sigma$   
534 confidence intervals reflect the sensitivity of the random sampling technique to uncertainties  
535 in time and space.

536 A number of low amplitude (decimetre-scale) sea-level changes are evident in the  
537 reconstruction, superimposed upon the millennial scale background trend. To isolate these  
538 deviations, we use the independent RSL reconstruction for the Cree Estuary of Bradley et al.  
539 (2011) as a threshold above which a sea-level event may be defined. This curve is derived  
540 from a solution to the sea-level equation (Mitrovica & Milne, 2003) with an updated  
541 deglacial history for the British and Irish Ice Sheet. The proximity of the site to the former  
542 centre of this ice sheet means that it is strongly affected by glacial isostatic adjustment, which  
543 is recorded in the RSL record. Since the Bradley et al. (2011) reconstruction is sampled at

544 1000 year time steps we choose to use this as our background sea-level curve. Using this  
545 background curve (and the rate one obtains by differentiating it) is a more conservative  
546 approach than using quadratic or cubic polynomials (e.g. Milliken et al., 2008) or partial  
547 linear segments either side of supposed sea-level jump (e.g. Hijma & Cohen, 2010) because it  
548 does not rely upon the RSL data itself to ascertain a background rate.

549 Fig. 7a plots rates of RSL change derived using the two methods outlined in Section  
550 3.4 (dataset presented in Table S3). For both mean RSL rate reconstruction ( $\mu_{dRSL/dt}$ ) and  
551 differentiated mean RSL reconstruction ( $d\mu_{RSL}/dt$ ) we observe a centennial-scale increase in  
552 the rate of RSL between ~8700-8300 cal yr BP that exceeds the background trend as defined  
553 by the Bradley et al. (2011). The fine structure of these differentiated records allow this event  
554 to be separated into two episodes, with a first commencing at ~8700 cal yr BP and a second  
555 at ~8560 cal yr BP. Third, we observe relatively minor fluctuations in rates of rise beyond the  
556 background threshold between the 8250-8150 cal yr BP time period. Importantly, these  
557 events correspond in time to the increases in SWLI within the raw reconstruction data and  
558 can therefore not be considered artefacts of the probabilistic assessment.

559 Determining precise estimates of the timing and magnitude of sea-level changes in the  
560 critical interval is difficult given the nature of our dataset and its uncertainties. Clear  
561 limitations exist in developing sub-centennially resolved sea-level histories from macrotidal  
562 settings, since the uncertainties in transfer-function derived RSL reconstructions are typically  
563 10% of the tidal range (Barlow et al., 2013). Each RSL data point also accounts for  
564 uncertainties relating to palaeotidal change ( $\pm 0.2$  m) and compaction ( $\pm 0.2$  m). Nevertheless  
565 we choose to proceed with reconstructing the timing and magnitudes of these events more  
566 precisely, using data around the mean, given the compelling evidence of marsh drowning  
567 within the stratigraphy. To achieve this, we utilise our differentiated RSL curves ( $d\mu_{RSL}/dt$ ).

568 Here we test hypothesis (1) with the following criterion: where rates of rise in the  
569 three differentiated RSL curves ( $d\mu_{RSL}/dt$ ,  $d(\mu-\sigma)_{RSL}/dt$ ,  $d(\mu+\sigma)_{RSL}/dt$ ) exceed the background  
570 rate (Bradley et al. 2011). The crossing time of each differentiated curve allows a simple  
571 range to be calculated for the onset of a sea-level event. Applying this criterion, we identify  
572 three accelerations in the rate of RSL rise (Table 3). The first occurred between 8760-8640  
573 cal yr BP and registered a sea-level jump of 0.24-0.45 m ( $RSLr_1$ ), while the second was at  
574 8595-8465 cal yr BP and registered 0.67-0.73 m ( $RSLr_2$ ). The final event registered 0.37-0.43  
575 m of sea-level rise within the period 8320-8235 cal yr BP (all ranges are  $3\sigma$  of the  
576 differentiated series).

577 We establish the total mass loss from each of these events by scaling the associated  
578 local RSL change by the percentage of global sea-level (GSL) equivalent predicted by  
579 Kendal et al. (2008) at the measurement site (Table 2). We perform this scaling by assuming  
580 a North American source (Fig. 1) and that the sea-level fingerprint is invariant to the  
581 magnitude of mass change so long as the geometry is the same. While in the Cree Estuary  
582 and Rhine-Meuse Delta, RSL is predicted to record 70% of the GSL equivalent change, the  
583 Mississippi Delta RSL would only record 20%.

584

## 585 **5. Discussion**

### 586 **5.1 Assessing the evidence for sea-level jumps in the Blair's Croft record**

587

588 We infer the RSL significance of abrupt microfossil changes by considering supporting  
589 (stratigraphic) evidence of abrupt drowning and whether these could reflect local  
590 morphodynamical processes. In turn, we assess the global sea-level significance of the Cree  
591 observations.

592 On the basis that abrupt microfossil changes are supported by lithostratigraphic  
593 evidence, in particular abrupt switches from organogenic to minerogenic sedimentation, we  
594 accept  $RSL_{R1}$  and  $RSL_{R3}$  as significant RSL jumps (Table 3). The notion that  $RSL_{R2}$  is a  
595 genuine short-lived event rests heavily on the interpretation of the relatively barren  
596 'planktonic zone'; a 45 cm unit containing only two samples of planktonic microfossils.  
597 Critically, the stratigraphy below the planktonic zone contains evidence of minor marsh  
598 recovery in the form of increased abundance of well-humified organic macrofossils and is in  
599 line with the interpretation that our marsh was experiencing recovery after a preceding sea-  
600 level jump ( $RSL_{R1}$ ). We therefore interpret the overlying planktonic zone as a drowning of a  
601 high mudflat or lower salt marsh environment that was in the early stages of vegetational  
602 recolonization. Moreover, our decision to introduce 'boundaries' within the age model at  
603 organogenic-minerogenic contacts will not have influenced the results from this section of  
604 core. Secondly, low marsh benthic microfossils (*Cocconeis scutellum*) increase in abundance  
605 immediately above and below the planktonic zone, demonstrating that accumulation kept  
606 pace within a sustained, sub-centennial to multi-decadal period where accommodation space  
607 was made available. In turn this line of evidence is not consistent with the notion that tidal

608 scour or a high-energy event such as a storm (e.g. Haslett and Bryant, 2007) as the  
609 microfossil record reflects gradual changes instead of abrupt transitions associated with  
610 erosion (Fig. 6). Third, supporting evidence of lagoonal infilling in response to enhanced  
611 freshwater runoff, such as laminations or freshwater taxa, are not present either within or  
612 above and below this unit. A further key observation is provided by Smith et al. (2003a), who  
613 describe an unprecedented increase in clay content at Carsewalloch Flow towards the centre  
614 of the estuary (Fig. 3C) between 4.0-4.5 m OD. Its elevation is similar to the elevation of the  
615 planktonic zone in BC421 (4.90-4.45 m OD) albeit slightly lower, likely reflecting less  
616 compaction of the valley side sediments at our site. We therefore suggest that the planktonic  
617 zone in BC421 records a shift in sedimentology that extends beyond Blair's Croft towards the  
618 centre of the estuary. We propose that the lack of a distinct organogenic-minerogenic  
619 lithostratigraphic signature similar to that observed for RSL<sub>r1</sub> and RSL<sub>r3</sub> can be explained by  
620 the low intertidal height of the pre-drowned surface (high mudflat or low salt marsh). The  
621 Solway Firth and its sub-estuaries contain an abundance of fine-grained sediment, which  
622 likely supported rapid sedimentation once accommodation space was made available by  
623 sudden sea-level rise. On these grounds, we conclude that there is strong evidence that RSL<sub>r2</sub>  
624 was a genuine RSL jump.

625         There are other possible explanations for the drowning events identified in the Blair's  
626 Croft sequence that could be of local origin and which require consideration. First,  
627 meandering tidal creeks could alter the local depositional environment and result in changes  
628 in diatom assemblages within the sample core. We dismiss this possibility on the basis that  
629 channel deposits are usually distinct within the litho- and biostratigraphy (e.g. Long and  
630 Innes, 1993; Zecchin et al., 2014) and do not operate over the wide areas in which the Blair's  
631 Croft organic beds are observed. A second possibility is that the local site stratigraphy may  
632 record changes in coastal morphodynamics associated with the development of a coastal  
633 barrier. This is potentially important when considering the RSL significance of the final event  
634 (RSL<sub>r3</sub>), which is derived from an exceptionally noisy part of the record. The site-wide  
635 stratigraphy that overlies this upper section of core is complex, with interweaving organic-  
636 minerogenic deposits that cannot be traced laterally in all cores. As noted above, the site  
637 chronology indicates that a gravel barrier was deposited at its present position sometime  
638 before c. 8000 cal yr BP. We find no stratigraphic evidence for changes in the dynamics of  
639 this barrier during the timeframe of our record, such as barrier over-wash deposits or  
640 evidence for tidal inlet deposition. However, we cannot rule out the control of barrier  
641 morphodynamics on the development of the latter stages of the record. For instance, Smith et

642 al. (2003a) describe evidence of a further two barrier ridges on the opposite side of the  
643 estuary of a similar morphology and this probably attests to the abundance of glacial  
644 sediment now buried within the valley lowlands. By the same token, a gravel barrier at the  
645 site would have provided a degree of protection for low energy conditions in its lee after c.  
646 8000 cal yr BP until the culmination of the RSL highstand in the region.

647 A final observation is that rates of RSL rise determined from sediments across the  
648 middle and upper organic beds are low. There is a gradual slowdown in the rate of long-term  
649 RSL rise across the interval that eventually falls short of the background trend as derived  
650 from Bradley et al. (2011) model. Plausibly, this might be explained by the long-term  
651 overburden pressure and the reduction in the thickness of the organic beds, suggesting that  
652 estimates of RSL rise may be underestimated. As organic (saltmarsh) sediments experience a  
653 greater degree of compressibility than minerogenic (mudflat) sediments (e.g., Brain et al.  
654 2011) we can assume that  $RSLr_2$  is unaffected by the impact of compression variability  
655 across lithologies as it is recorded within a single minerogenic silt. On the other hand,  $RSLr_1$   
656 and  $RSLr_3$  directly overlie the lower and middle beds and their onsets occur at or near the  
657 organogenic-minerogenic contacts. Whilst we cannot quantify the influence of compaction,  
658 the microfossil changes observed are independent of potential compaction variability across  
659 lithologies. Hence, we conclude that there is evidence that RSL rose in three steps prior to the  
660 8.2 event and are therefore unable to reject hypothesis (1), that RSL rose in more than one  
661 abrupt step in the centuries leading up to the 8.2 event.

662

## 663 **5.2 Comparison with existing chronologies: testing hypothesis (2)**

664

665 There is debate regarding the potential routing and impact of freshwater discharge at the time  
666 interval of interest, with some authors suggesting routing into the sub-tropical North Atlantic  
667 and not the sub-polar gyre (e.g. Condron and Windsor 2011; Hill and Condron, 2014).  
668 Nevertheless, the strong polar foraminiferal and  $\delta^{18}O$  signal in records from the sub-polar  
669 North Atlantic (Ellison et al., 2005; Kleiven et al., 2008) indicates a significant impact in this  
670 region and provides a basis for chronological comparison with the three Cree Estuary RSL  
671 jumps.

672 Fig. 8 plots the age probability density functions and  $2\sigma$  ranges (bars) computed for  
673 the start of each respective North Atlantic event. We observe ages that cluster in three largely

674 distinct time intervals, with mid-points that are separated by up to two centuries. A first group  
675 contains RSL<sub>r1</sub>, DCP6a and modelled peak meltwater discharge concomitant with LIS saddle  
676 collapse, which all occur between ~8800 to ~8600 cal yr BP. A second group of events  
677 contains RSL<sub>r2</sub>, DCP6b; the downstream equivalent of the Hudson Bay “red-bed”, the Rhine-  
678 Meuse Delta RSL jump and the earliest North Atlantic surface freshening event (FE<sub>1</sub>) in  
679 MD99-2665, which occur between ~8600 to ~8300 cal yr BP. The final group of events  
680 occurred between ~8300 and ~8100 cal BP, where RSL<sub>r3</sub>, the Mississippi Delta RSL jump  
681 and the youngest North Atlantic surface freshening event (FE<sub>2</sub>) in MD99-2665 indicate  
682 strong overlap at the 1 $\sigma$  probability level. The 2 $\sigma$  range of DCP7 (Jennings et al., 2015) and  
683 the LAO drainage deposit recorded in James Bay (Roy et al., 2010) overlaps with the 2 $\sigma$   
684 range of this final age group. In addition, they all overlap with the start of the 8.2 event at  
685 8247 cal yr BP (Thomas et al. 2007). Table 2 provides the age determinations of these  
686 individual estimates.

687         Interpreting an accurate sequence of freshwater events is strongly dependent on the  
688 accuracy of the underpinning chronologies. Maximising chronological accuracy and precision  
689 is critical given the short timescale under consideration and because of the limitations  
690 imposed by variable <sup>14</sup>C production across the time interval. In particular, minor plateaus in  
691 <sup>14</sup>C production occur between 8550-8400, 8300-8200 and 8150-8050 cal yr BP, while a much  
692 larger plateau occurs at 8950-8650 cal yr BP and could be implicated in the strong  
693 correlations in Fig. 8. To some extent however, this potential biasing effect is mitigated  
694 where age models incorporate stratigraphic information; such is the case with the Cree  
695 record. However, our age model contains the assumption that sharp changes from organic to  
696 minerogenic sedimentation reflect a changing rate of accumulation. Our introduction of  
697 “boundaries” at these contacts effectively forces the model to derive a solution that is  
698 otherwise not possible given our dating constraints and nature of the stratigraphic sequence.  
699 Validation of our observations is therefore required, especially with respect to time  
700 constraints. As a final point, the estimates derived from marine chronologies presented here  
701 depend strongly on the magnitude of local marine reservoir corrections which are difficult to  
702 define. These limitations are inherent to the process of <sup>14</sup>C calibration but are compounded  
703 when working on these timescales. Notwithstanding these issues we suggest that events are  
704 likely to have been interrelated in some way when ages overlap, especially at the 1 $\sigma$   
705 probability level.

706 The Cree observations demonstrate significant overlap in timing with existing  
707 estimates of short-lived events (Fig, 8); in particular those within the best resolved near-field  
708 record of final LIS retreat on the Cartwright Saddle (Jennings et al., 2015), but also from the  
709 two existing RSL records that span the critical time interval. After correcting  $RSLr_1$  and  
710  $RSLr_2$  for a Laurentide source of freshwater release,  $RSLr_1$  measured 0.35-0.65 m while  
711  $RSLr_2$  measured 0.96-1.04 m. This is in good agreement with the fingerprint-corrected sea-  
712 level jump observed in the in the Rhine-Meuse Delta of  $3.0 \pm 1.3$  m ( $1\sigma$ ; Hijma and Cohen,  
713 2010). It has been speculated that the Rhine-Meuse RSL jump records two or more distinct  
714 events (Hijma and Cohen, 2010; Li et al., 2012), a suggestion that is in agreement with our  
715 data after considering the magnitudes of  $RSLr_1$  and  $RSLr_2$  once combined (1.92-2.23 m)  
716 (Table 2). Thus, there is compelling evidence to support an interpretation that two episodes of  
717 freshwater release occurred in quick succession, and that these their distinct separation has  
718 yet to be fully detected in the Rhine-Meuse Delta sea-level record (Hijma and Cohen, 2010).  
719 Finally, the magnitude of  $RSLr_3$  once corrected for a Laurentide source of freshwater release  
720 (0.54-0.61 m) is in good agreement with the magnitude of the fingerprint-corrected RSL  
721 jump identified in the Mississippi Delta ( $0.3 \pm 0.3$  m;  $2\sigma$ ; Li et al., 2012).

722

### 723 **5.3 Deriving a sequence of events between 8900 to 8200 cal yr BP**

724

725 In light of the Cree and existing observations, we propose the following three-event model of  
726 freshwater forcing from the LIS between 8900-8200 cal yr BP.

727 First, collapse of the Keewatin and Labrador ice-dome saddle (Gregoire et al., 2012)  
728 was swiftly followed by the opening of the Tyrrell Sea (Jennings et al., 2015). It coincides  
729 closely with detrital carbonate event DCP6a in core MD99-2236 from the Cartwright Saddle,  
730 dated to 8694-8609 cal yr BP (Jennings et al. 2015). This first event at ~8700 cal yr BP  
731 registered a RSL rise in SW Scotland of 0.25-0.45 m, which translates to a eustatic-  
732 equivalent magnitude of 0.35-0.65 m. There is no evidence of this event within sub-polar  
733 North Atlantic proxy records which could reflect low rates of freshwater discharge during  
734 this event, relative to the events that followed. However, it overlaps with a possible cold  
735 event at 8.75 ka BP exemplified by Rasmussen et al. (2007) in Greenland ice-core records. It  
736 could also have been responsible for the onset of the broad climatic anomaly that starts  
737 around this time (Rohling and Pälike, 2005).

738           A second episode of enhanced freshwater forcing followed shortly after at ~8560 cal  
739 yr BP and this registered a surface and deep ocean signal (FE<sub>1</sub>; Kleiven et al., 2008; Ellison et  
740 al., 2005 Fig. 2) along with RSL jumps in SW Scotland (RSL<sub>2</sub>) and the western Netherlands.  
741 It was likely responsible for the reworked stratigraphy in the Mississippi Delta record (Li et  
742 al., 2012). The event agrees in timing with DCP6b, which Jennings et al. (2015) date to 8609-  
743 8489 cal yr BP and correlate with the Hudson Bay “red bed” deposit (e.g. Barber et al.,  
744 1999). We propose that RSL<sub>2</sub> records the first and largest drainage of LAO. As it swiftly  
745 followed RSL<sub>1</sub>, we suggest that the collapse of the Keewatin and Labrador ice-domes  
746 reached a critical threshold whereby sufficient thinning forced the drainage of LAO  
747 subglacially under buoyant ice (Lajeunesse and St Onge, 2008; Clarke et al., 2004; Teller et  
748 al., 2002). The notion of a negligible time gap between these two events is supported by two  
749 lines of evidence; first, DCP6 has been subdivided into two remarkably close but largely  
750 separate events (DCP6a and DCP6b) by Jennings et al. (2015). Second, the Rhine-Meuse  
751 Delta RSL record (Hijma and Cohen, 2010) was unable to capture two distinctly separate  
752 events.

753           The final event within the Cree Estuary (RSL<sub>3</sub>) occurred between 8323-8218 cal yr  
754 BP and correlates broadly with DCP7; dated to 8219-7998 cal yr BP, which Jennings et al.  
755 (2015) interpret as representing the possible two-staged release of LAO and the cause of the  
756 8.2 event. The LIS was the most likely source of this event given its registration in sub-polar  
757 North Atlantic proxy records (Ellison et al. 2006; Kleiven et al., 2008). It is therefore unlikely  
758 that the majority of freshwater was routed south into the sub-tropical gyre (Condrón and  
759 Windsor, 2011; Hill and Condrón, 2014), although it remains possible that this region  
760 received a portion of the total discharge volume. In view of the James Bay drainage deposits,  
761 which provide strong overlap at the 1 $\sigma$  probability level (Roy et al. 2011), we interpret this  
762 event as the second and final drainage of LAO following a century-scale phase of partial lake  
763 recharge (Teller et al., 2002).

764           The differences in the magnitudes of RSL jumps have implications for AMOC  
765 sensitivity. The relatively large and abrupt freshwater pulses at ~8700 and ~8560 cal yr BP  
766 associated with the opening of the Tyrrell Sea and first drainage of LAO respectively could  
767 have preconditioned the AMOC (e.g. Carlson and Clark, 2012), with a relatively modest  
768 freshwater perturbation at ~8270 yrs BP triggering its eventual reorganization. Thereafter, it  
769 is possible that sea-ice-albedo feedbacks (Wiersma and Jongma, 2010; Otto-Bliesner and



770 Brady, 2010) and freshwater fluxes were important in forcing the 8.2 event (Teller et al.,  
771 2002; Törnqvist and Hijma, 2012).

772

## 773 **6. Conclusions**

774

775 The exceptionally well-mapped 8.2 event was originally thought to have been triggered by an  
776 AMOC freshwater perturbation associated with the drainage of LAO, but studies based on  
777 empirical data and modelling have increasingly speculated that the single-event model of  
778 freshwater forcing is an oversimplification of the 8.2 event's causal mechanism. RSL records  
779 provide one of the few means to calculate the magnitude of freshwater released and to  
780 determine a likely sequence of freshwater events prior to the 8.2 event.

781 We present the first microfossil-based RSL record that is continuous from 8800 to  
782 7800 cal yr BP. It contains three decimetre- to metre-scale RSL jumps that overlap in age  
783 with a range of abrupt events expressed in existing North Atlantic records, lending significant  
784 support to a three-event model of Laurentide freshwater release within the c. 500 yr window  
785 prior to the 8.2 event.

786 Our observations agree with a two-event model of LAO drainage which was preceded  
787 by a dynamical ice-sheet contribution at ~8650 cal yr BP (0.35-0.65 m). The first  
788 (penultimate) drainage was at ~8565 cal yr BP (0.96-1.04 m), while the final appears coeval  
789 with the start of the 8.2 event. Our observations demonstrate the potential offered by  
790 integrating ice core, ocean and coastal records of environmental change across this turbulent  
791 interval of the Holocene, whilst also highlighting the challenges posed by developing  
792 continuous records from single stratigraphic sequences that rely heavily on the radiocarbon  
793 method. Developing additional highly resolved RSL records of the type developed here,  
794 preferably from low tidal range settings and from southern Hemisphere settings to assist in  
795 fingerprinting sources and magnitudes of sea-level change, will enable further testing of the  
796 hypotheses that lie at the heart of this study.

797

## 798 **Acknowledgements**

799 Funding for this work was provided by a Durham Doctoral Award to TL. Hatfield College  
800 and the Hatfield College Trust are kindly acknowledged for fieldwork support. Radiocarbon

801 dating support comes from the Natural Environmental Research Council Radiocarbon  
802 Committee, allocation #1629.0312. We thank Drs. Sarah Bradley, Anne Jennings and Sophie  
803 Ward for providing and discussing various datasets and Professor Eelco Rohling for  
804 clarifying the probabilistic assessment method. This work benefitted from discussions with  
805 Drs. Lauren Gregoire, Sarah Woodroffe, James Wells and Professor Ian Shennan. We are  
806 grateful to Scott Rexworthy and Josh Kittlety for their assistance in the field and Mervyn  
807 Brown, Frank Davies, Alison George and Kathryn Melvin for technical and laboratory  
808 assistance. The reviews of Professor Torbjorn Törnqvist and an anonymous reviewer greatly  
809 improved an earlier version of the manuscript. This paper is a contribution to PALSEA2,  
810 IGCP 588 and the INQUA Commission on Coastal and Marine Processes.

811

## 812 **References**

- Alley, R. B., P. A. Mayewski, T. Sowers, M. Stuiver, K. C. Taylor, and P. U. Clark (1997),  
Holocene climatic instability: A prominent, widespread event 8200 yr ago, *Geology* **25**,  
483–486.
- Alley, R.B and Agustdottir, A.M. 2005. The 8k event: causes and consequences of a major  
Holocene abrupt climate change, *Quaternary Science Reviews* **24**, 1123-1149.
- Barber, D.C., Dyke, A., Hillaire-Marcel, C., Jennings, A.E., Andrews, J.T., Kerwin, M.T.,  
Bilodeau, G., McNeely, G., Southon, J., Morehead, M.D., and Gagnon, J.-M. 1999.  
Forcing of the cold event of 8,200 years ago by catastrophic drainage of Laurentide  
lake: *Nature* **400**. 344–348, doi: 10.1038/22504.
- Barlow N. L. M., Shennan I., Long A.J., Gehrels, W.R., Saher, M.H., Woodroffe, S.A.,  
Hillier, C. H. 2013. Salt marshes as late Holocene tide gauges. *Global and Planetary  
Change* **106**, 90–110.
- Birks, H.J.B., 1995. Quantitative palaeoenvironmental reconstructions. In: Maddy, D., Brew,  
J.S. (Eds.), *Statistical Modelling of Quaternary Science Data*. Quaternary Research  
Association, Cambridge, 161–254.
- Bishop, W. W. & Coope, G. R. 1977. Stratigraphical and faunal evidence for Lateglacial and  
early Flandrian environments in south-west Scotland. In Gray, J. M. & Lowe, J. J.  
(eds), *Studies in the Scottish Late glacial environment*, 61±88. Oxford: Pergamon Press.
- Bondevik, S., Stormo, S.K., Gudrun, S. 2012. Green mosses date the Storegga tsunami to the  
chilliest decades of the 8.2 ka cold event, *Quaternary Science Reviews* **45**, 1-6.  
doi:10.1016/j.quascirev.2012.04.020.
- Bradley, S.L., Milne, G.A., Shennan, I., and Edwards, R. 2011. An improved Glacial  
Isostatic Adjustment model for the British Isles, *Journal of Quaternary Science* **26**, 5,  
541-552.

- Brain, M.J., Long, A.J., Petley, D.N., Horton, B.P. and Allison, R.J. Compression behaviour of minerogenic low energy intertidal sediments. *Sedimentary Geology* **233**, 28-41.
- Bronk Ramsey, C. 2000. Comment on 'The Use of Bayesian Statistics for 14C dates of chronologically ordered samples: a critical analysis'. *Radiocarbon*, **42**, 2, 199-202.
- Bronk Ramsey, C. 2008. Deposition models for chronological records. *Quaternary Science Reviews*, **27**, 1-2, 42-60.
- Bronk Ramsey, C. 2008. Deposition models for chronological records. *Quaternary Science Reviews*, **27**, 1-2, 42-60.
- Bronk Ramsey, C. 2009. Bayesian analysis of radiocarbon dates. *Radiocarbon*, **51**, 1, 337-360.
- Carlson, A.E., and Clark, P.U., 2012, Ice-sheet sources of sea-level rise and freshwater discharge during the last deglaciation, *Reviews of Geophysics* **50**, doi: 10.1029/2011RG000371.
- Clarke, G. K. C., Leverington, D. W., Teller, J. T. & Dyke, A. S. 2004. Paleohydraulics of the last outburst flood from glacial Lake Agassiz and the 8200 BP cold event. *Quaternary Science Reviews* **23**, 389–407.
- Condron, A., Windsor, P. 2011. A subtropical fate awaited freshwater discharged from glacial Lake Agassiz, *Geophysical Research Letters* **38**, 3, 10.1029/2010GL046011.
- Cullingford, R. A., Caseldine, C. J. and Gotts, P. E. 1980. Early Flandrian land and sea level changes in Lower Strathearn. *Nature* **284**, 159-61.
- Czernik, J., Goslar, T. 2001. Preparation of graphite targets in The Gliwice Radiocarbon Laboratory for AMS 14C dating. *Radiocarbon* **43**, 283–291.
- de Vernal, A., Hillaire-Marcel, C., von Grafenstein, U., Barber, D., 1997. Researchers look for links among paleoclimate events: EOS (Transactions, American Geophysical Union) **78**, 247–249.
- Ellison, C.R.W., Chapman, M.R., and Hall, I.R. 2006. Surface and deep ocean interactions during the cold climate event 8200 years ago. *Science* **312**, 1929–1932, doi: 10.1126/science.1127213.
- Gehrels W.R., Kirby J.R., Prokoph A., *et al.* 2005. Onset of recent rapid sea-level rise in the western Atlantic Ocean. *Quaternary Science Reviews* **24**: 2083–2100.
- Gehrels, W.R., Roe, H.M., Charman, D.J. 2001. Foraminifera, testate amoebae and diatoms as sea-level indicators in UK saltmarshes: a quantitative multiproxy approach, *Journal Quaternary Science* **16**, 3, 201-220. DOI: 10.1002/JQS.588.
- Gilks, W., Richardson, S., Spiegelhalter, D. (Eds.) 1996. Markov Chain Monte Carlo in Practice. Chapman & Hall, London.

- Gregoire, L. J., Payne, A. J., Valdes, P. J. 2012. Deglacial rapid sea level rises caused by ice-sheet saddle collapses, *Nature* **487**, 219–222.
- Hartley, B., Barber, H.G., Carter, J.R. 1996. An Atlas of British Diatoms. Sims, P.A (ed). Biopress, London.
- Haslett, S.K., and Bryant, E.A. 2007. Reconnaissance of historic (post-AD 1000) high-energy deposits along the Atlantic coasts of southwest Britain, Ireland and Brittany, France. *Marine Geology* **242**, 207-220.
- Hijma, M.P and Cohen, K.M. 2010. Timing and magnitude of the sea-level jump precluding the 8200 yr event, *Geology* **38**, 3, 275-278.
- Hill, J.C., Condrón, A. 2014. Subtropical iceberg scours and meltwater routing in the deglacial western North Atlantic, *Nature Geoscience* **7**, 806-810. DOI: 10.1038/NGEO2267.
- Hill, T.C.B., Woodland, W.A., Spencer, C.D., and Marriot, S.B. 2007. Holocene sea-level change in the Severn Estuary, southwest England: a diatom-based sea-level transfer function for macrotidal settings. *The Holocene*, **17**, 5, 639-648.
- Hillaire-Marcel, C. de Vernal, A. Piper, D.J.W. 2007. Lake Agassiz final drainage event in the North Atlantic. *Geophysical Research Letters* **34**, doi:10.1029/2007GL030396.
- Hoffman, A.S., Carlson, A.E., Windsor, K., Klinkhammer, G.P., Le Grande, A.N., Andrews, J.T., Strasser, J.C. 2012. Linking the 8.2 ka event and its freshwater forcing in the Labrador Sea, *Geophysical Research Letters* **39**, doi:10.1029/2012GL053047.
- Hydrographic Office (2011) Admiralty Tide Tables: United Kingdom and Ireland including European and Channel Ports: Hydrographer of the Navy, Taunton, Somerset, 1, 1-364.
- Jardine, W. G. 1975. Chronology of Holocene marine transgression and regression in southwestern Scotland. *Boreas* **4**, 173-96.
- Jennings, A., Andrews, J., Pierce, C., Wilson, L., Olfasdottir, S. 2015. Detrital carbonate peaks on the Labrador shelf, a 13e7 ka template for freshwater forcing from the Hudson Strait outlet of the Laurentide Ice Sheet into the subpolar gyre, *Quaternary Science Reviews* **107**, 62-80. <http://dx.doi.org/10.1016/j.quascirev.2014.10.022>.
- Juggins, S. (2011) C<sup>2</sup> Version 1.6: Software for Ecological and Palaeoecological Data Analysis and Visualisation: Department of Geography, University of Newcastle, Newcastle upon Tyne, U.K.
- Kendall, R.A, Mitrovica, J.X., Milne, G.A., Tornqvist, T.E. and Li, Y.X. 2008. The sea-level fingerprint of the 8.2 ka event, *The Geological Society of America* **35**, 5, 423-426.
- Kleiven, H.F., Kissel, C., Laj, C., Ninnemann, U.S., Richter, T.O., Cortijo, E. 2008. Reduced North Atlantic deep water coeval with the glacial Lake Agassiz Freshwater Outburst. *Science* **319**, 5859, 60-64.

- Kobashi, T., Severinghaus, J.P., Brook, E.J., Barnola, J.M., and Grachev., A.M. 2007. Precise timing and characterization of abrupt climate change 8200 years ago from air trapped in polar ice. *Quaternary Science Reviews* **26**, 1212–1222, doi:10.1016/j.quascirev.2007.01.009.
- Kuchar, J., Milne, G., Hubbard, A., Patton, H., Bradley, S., Shennan, I., and Edward, R. 2012. Evaluation of a numerical model of the British-Irish ice sheet using relative sea-level data: implications for the interpretation of trimline observations, *Journal Quaternary Science* **27**, 6, 597-605.
- Lajeunesse, P., and St-Onge, G. The subglacial origin of the Lake Agassiz-Ojibway final outburst flood, *Nature Geoscience* **1**, 184-187. doi:10.1038/ngeo130.
- LeGrande, A.N., Schmidt, G.A., Shindell, D.T., Field, C.V., Miller, R.L., Koch, D.M., Faluvegi, G. and Hoffman, G. 2006. Consistent simulations of multiple proxy responses to an abrupt climate change event, *Proceedings of the National Academy of Sciences* **103**, 4, 837-842. doi: 10.1073/pnas.0510095103.
- Leverington, D. W., J. D. Mann, and J. T. Teller. 2002. Changes in the bathymetry and volume of glacial Lake Agassiz between 9200 and 7700 14C yr B.P. *Quaternary Research* **57**, 244–252.
- Li, Y.X., Tornqvist, T.E., Nevitt, J.M., and Kohl, B. 2011. Synchronizing a sea-level jump, final lake Agassiz drainage and abrupt cooling 8200 years ago, *Earth and Planetary Science Letters* **315-316**, 41-50.
- Lloyd,, J.M., Shennan, I., Kirby, J.R. and Rutherford, M.M. 1999. Holocene relative sea – level changes in the inner Solway Firth. *Quaternary International* **60**, 83-105.
- Long, A.J. and Innes, J.B. 1993. Holocene sea-level and coastal sedimentation in Romney Marsh, southeast England, UK. *The Proceedings of the Geologists' Association*, 104, 223-237.
- Marshall, W.A., Gehrels, W.R., Garnett, M.H., Freeman, S.P.H.T., Maden, C., Xu, S., 2007. The use of ‘bomb spike’ calibration and high-precision AMS 14C analyses to date salt-marsh sediments deposited during the past three centuries. *Quaternary Research*, **68**, 325–337.
- Mitrovica, J.X., Gomez, N., Clark, P.U. 2009. The sea-level fingerprint of West Antarctic collapse, *Science* **323**, 753.
- Mitrovica, J.X. and Milne, G.A. 2003. On post-glacial sea level: I. General theory. *Geophysical Journal International*, 154: 253–267. doi: 10.1046/j.1365-246X.2003.01942.x
- Mitrovica, J.X., Tamisiea, M.E., Davis, J.L., Milne, G.A. 2001. Recent mass balance of polar ice sheets inferred from patterns of global sea-level change, *Nature* **409**, 1026-1029.
- Morrill, C., Ward, E.M., Wagner, A.J., Otto-Bliesner, B.L., Rosenbloom, N. 2014. Large sensitivity to freshwater forcing location in 8.2 ka simulations. *Paleoceanography* **29**, doi:10.1002/2014PA002669.

- Otto-Bliesner, B.I. and Brady, E.C. 2010. The sensitivity of the climate response to the magnitude and location of freshwater forcing: last glacial maximum experiments, *Quaternary Science Reviews* **29**, 56-73.
- Palmer, A.J.M., and Abbott, W.H. 1986. Diatoms as sea-level indicators. In: Van de Plassche O (ed) *Sea level research: A manual for the collection and evaluation of data*. Geo Books, Norwich.
- Rasmussen, S. O., Seierstad, I. K., Andersen, K. K., Bigler, M., Dahl-Jensen, D., and Johnsen, S. J 2008. Synchronization of the NGRIP, GRIP, and GISP2 ice cores across MIS 2 and palaeoclimatic implications, *Quaternary Science Reviews* **27**, 18–28, doi:10.1016/j.quascirev.2007.1001.1016.
- Reimer, P. J., Bard, E., Bayliss, A., Beck, J. W., Blackwell, P. G., Bronk Ramsey, C., Grootes, P. M., Guilderson, T. P., Haflidason, H., Hajdas, I., HattĹ, C., Heaton, T. J., Hoffmann, D. L., Hogg, A. G., Hughen, K. A., Kaiser, K. F., Kromer, B., Manning, S. W., Niu, M., Reimer, R. W., Richards, D. A., Scott, E. M., Southon, J. R., Staff, R. A., Turney, C. S. M., & van der Plicht, J. 2013. IntCal13 and Marine13 Radiocarbon Age Calibration Curves 0-50,000 Years cal BP, *Radiocarbon* **55**.
- Rohling, E.J., Foster, G.L., Grant, K.M., Marino, G., Roberts, A.P., Tamisiea, M.E. and Williams, F. 2014. Sea-level and deep-sea temperature variability over the past 5.3 million years, *Nature* **508**, 477-482.
- Roy, M., Dell'Oste, F., Veillette, J.J., de Vernal, A., Helie, J.-F., Parent, M., 2011. Insights on the events surrounding the final drainage of Lake Ojibway based on James Bay stratigraphic sequences. *Quaternary Science Reviews* **30**, 682-692.
- Simkins, L.M., Simms, A.R., Cruse, A.M., Troiani, T. Atekwana, E.A., Puckette, J., Yokoyama, Y. 2012. Correlation of early and mid-Holocene events using magnetic susceptibility in estuarine cores from bays along the northwestern Gulf of Mexico, *Palaeogeography, Palaeoclimatology, Palaeoecology* **346-347**, 95-107.
- Smith, D.E., Wells, J.M., Mighall, T.M., Cullingford, R.A., Holloway, L.K., Dawson, S., Brooks, C.L. 2003a. Holocene relative sea levels and coastal changes in the lower Cree valley and estuary, SW Scotland, UK. *Transactions of the Royal Society of Edinburgh: Earth Sciences*, **93**, 301-331.
- Smith, D.E., Haggart, B.A., Cullingford, R.A., Tipping, R.M., Wells, J.M., Mighall, T.M. and Dawson, S. 2003b. Holocene relative sea level change in the lower Nith valley and estuary. *Scottish Journal of Geology* **39**, 97-120.
- Smith, D.E., Harrison, S. and Jordan, J.T. 2013. Sea level rise and submarine mass failures on open continental margins. *Quaternary Science Reviews* **82**, 93-103.
- Tamisiea ME, Mitrovica JX, Milne GA, Davis JL. 2003. Long wave length sea level and solid surface perturbations driven by polar ice mass variations: fingerprinting Greenland and Antarctic Ice Sheet flux. *Space Science Reviews* (108) 81–93.

- Teller, J. T., Leverington, D. W. & Mann, J. D. 2002. Freshwater outbursts to the oceans from glacial Lake Agassiz and their role in climate change during the last deglaciation. *Quaternary Science Reviews* **21**, 879–887.
- ter Braak, C.J.F., Juggins, S., 1993. Weighted averaging partial least squared regression (WA-PLS): an improved method for reconstructing environmental variables from species assemblages. *Hydrobiologia* **269**, 270, 485–502.
- Thomas, E.R., Wolff, E.W., Mulvaney, R., Steffensen, J.P., Johnsen, S.J., Arrowsmith, C., White, J.W.C., Vaughn, B., Popp, T. 2007. The 8.2 ka event from Greenland ice cores. *Quaternary Science Reviews* **26**, 1-2, 70-81.
- Törnqvist, T.E., Hijma, M.P. 2012. Links between early Holocene ice-sheet decay, sea-level rise and abrupt climate change, *Nature Geoscience* **5**, 601-606. DOI: 10.1038/NNGEO1536.
- Troels-Smith, J. 1955. Karakterisering af løse jordarter. Characterisation of unconsolidated sediments, *Geological Survey of Denmark*, **4**, 3, 1-73.
- Vos, Peter C., de Wolf, H., 1993. Diatoms as a tool for reconstructing sedimentary environments in coastal wetlands; methodological aspects. In: Twelfth International Diatom Symposium. Springer, Netherlands, 285-296.
- Ward, S. L., 2014. A new proxy for constraining palaeotidal model simulation of the Northwest European Shelf Seas. Doctoral thesis, Bangor University.
- Wells, J. M. 1997. *Flandrian relative sea level changes in the Cree estuary region, southwest Scotland*. Doctoral thesis. Coventry University.
- Wiersma AP, Renssen H. 2006. Model–data comparison for the 8.2 ka BP event: confirmation of a forcing mechanism by catastrophic drainage of Laurentide lakes. *Quaternary Science Reviews* **25**, 63–88.
- Wiersma, A.P., Jongma, J.I. 2010. A role for icebergs in the 8.2 ka climate event, *Climate Dynamics* **35**, 535-549.
- Wiersma, A.P., Roche, D.M., and Renssen, H. 2011. Fingerprinting the 8.2 ka climate response in a coupled climate model, *Journal Quaternary Science* **26**, 1, 118-127.
- Wilson, G.P., and Lamb, A.L. 2011. An assessment of the utility of regional diatom-based transfer functions. *Journal Quaternary Science* **27**, 4, 360-370. DOI: 10.1002/jqs.1553.
- Zecchin, M., Tosi, L., Caffau, M., Baradello, L., Donnici, S. 2014. Sequence stratigraphic significance of tidal channel systems in shallow lagoon (Venice, Italy). *The Holocene* **24**, 6. doi:10.1177/0959683614526903.
- Zong, Y. and Tooley, M.J. 1996. Holocene sea-level changes and crustal movements in Morecambe Bay, northwest England. *Journal of Quaternary Science* **11**(1), 43-58.

Zong, Y., Horton, B.P. 1999. Diatom-based tidal-level transfer functions as an aid in reconstructing Quaternary history of sea-level movements in the UK. *Journal Quaternary Science* **14**, 2, 153-167.



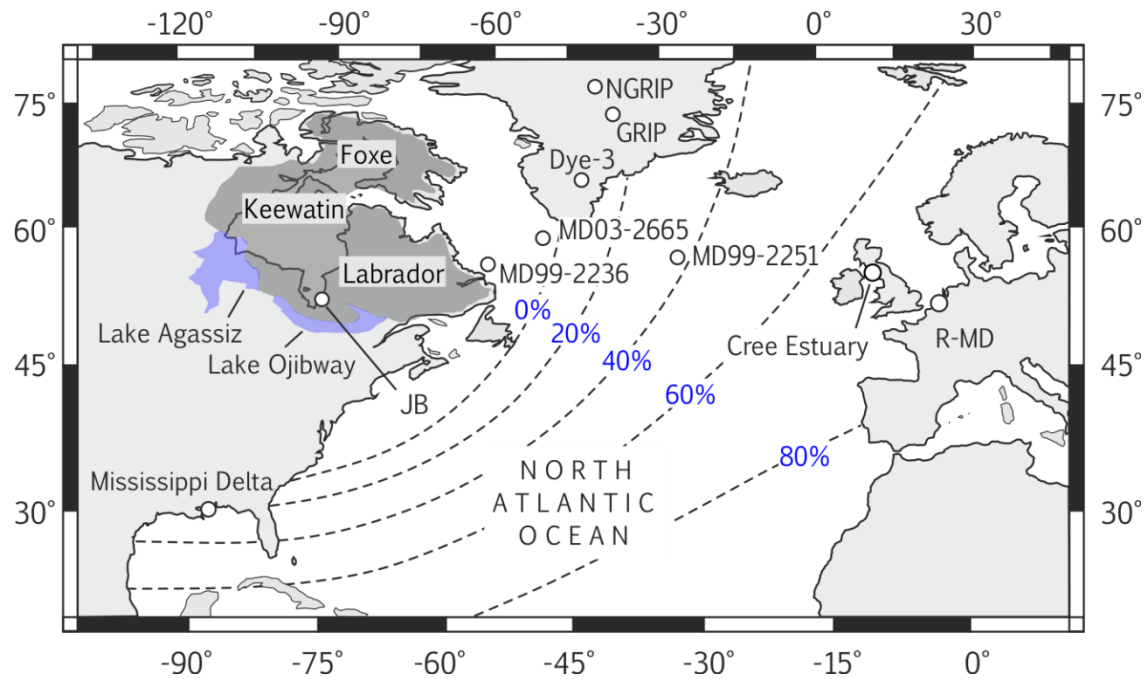


**Figure 1. Map of circum-North Atlantic with key locations mentioned in text.** Blue and dark grey shading indicates the approximate extent of Laurentide Ice Sheet and proglacial lakes Agassiz and Ojibway at ~8900 cal yr BP (after Dyke, 2004). Dashed lines denote the spatial variability of RSL rise associated with a LAO source of meltwater release from GIA modelling (after Kendall et al., 2008). JB = James Bay. R-MD = Rhine-Meuse Delta.

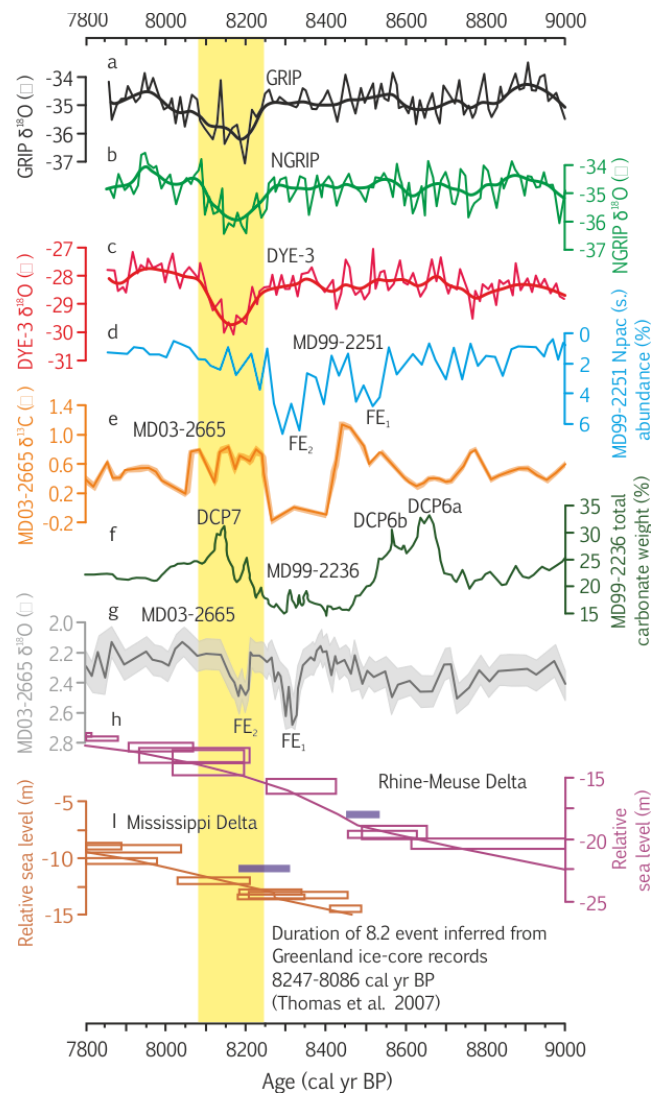


**Figure 2. Records of early Holocene climate, oceanographic and sea-level change in the North Atlantic.** Ages are calibrated with respect to AD 1950. **a**, GRIP  $\delta^{18}\text{O}$  with a 50 yr moving Gaussian smoothing. **b**, NGRIP  $\delta^{18}\text{O}$  with a 50 yr Gaussian smoothing **c**, Dye-3  $\delta^{18}\text{O}$  with a 50 yr Gaussian smoothing. **d**, *Neogloboquadrina pachyderma* (s.) abundance in North Atlantic deep sea sediments (Ellison et al., 2006). **e**, *Neogloboquadrina pachyderma* s.  $\delta^{13}\text{C}$  in Labrador Sea sea-floor sediments (Kleiven et al., 2008), on revised chronology (this study). FE<sub>1</sub> = Freshening Event 1; FE<sub>2</sub> = Freshening Event 2 (see text). **f**, Percentage detrital carbonate by weight in Cartwright Saddle sea-floor sediments (Jennings et al., 2015). DCP events correspond to ‘detrital carbonate peaks’. **g**, *Neogloboquadrina pachyderma* s.  $\delta^{18}\text{O}$  record in Labrador Sea sea-floor sediments (Kleiven et al., 2008), on its revised chronology (this study). FE<sub>1</sub> = Freshening Event 1; FE<sub>2</sub> = Freshening Event 2 (see text). **h**, Relative sea-level record from the Rhine-Meuse delta defined as  $2\sigma$  age and vertical uncertainty error boxes (Hijma and Cohen, 2010). Blue bar denotes  $2\sigma$  age range of the start of the RSL jump (Table 2). **i**, Relative sea-level record from the Mississippi Delta defined as  $2\sigma$  age and vertical uncertainty error boxes (Li et al., 2011). Blue bar denotes  $2\sigma$  age range that encompasses the RSL jump in its entirety (Table 2). Yellow bar indicates duration of the 8.2 event as inferred from a ‘stack’ of Greenland ice core records (Thomas et al., 2007).

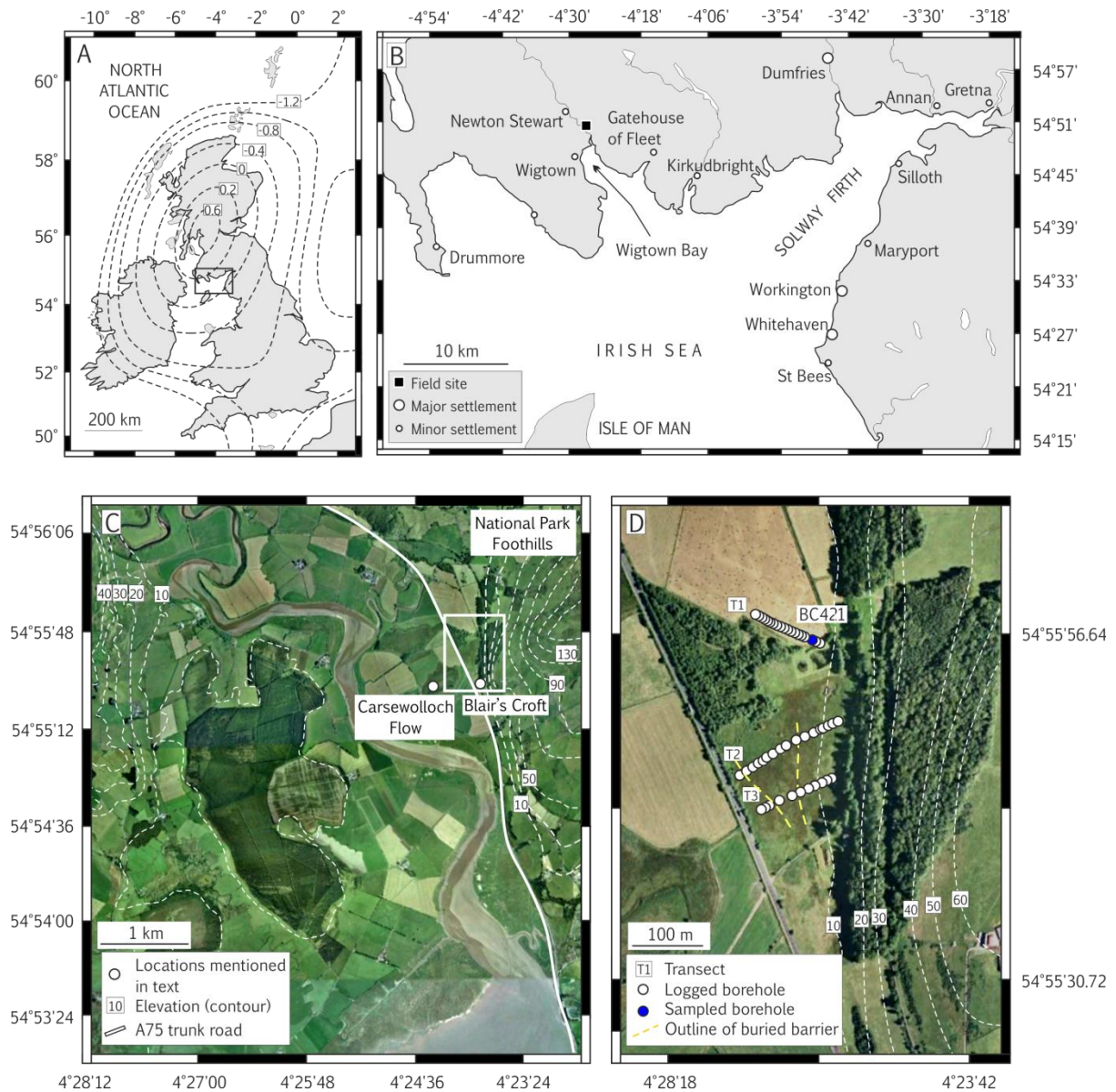


**Fig. 3.** Location maps of field site in southwest Scotland. A) Map of UK and Ireland overlain with the contour lines of the present-day vertical land motions determined by the glacio-isostatic adjustment model of Bradley et al. (2011), denoting uplift rates in  $\text{mm yr}^{-1}$ . B) Setting of Solway Firth in the Irish Sea and the location of Wigtown Bay and the Cree Estuary. C) Google Earth image of the Cree Lowlands and locations mentioned in text. D) Google Earth overview of Blair's Croft field-site and borehole locations.

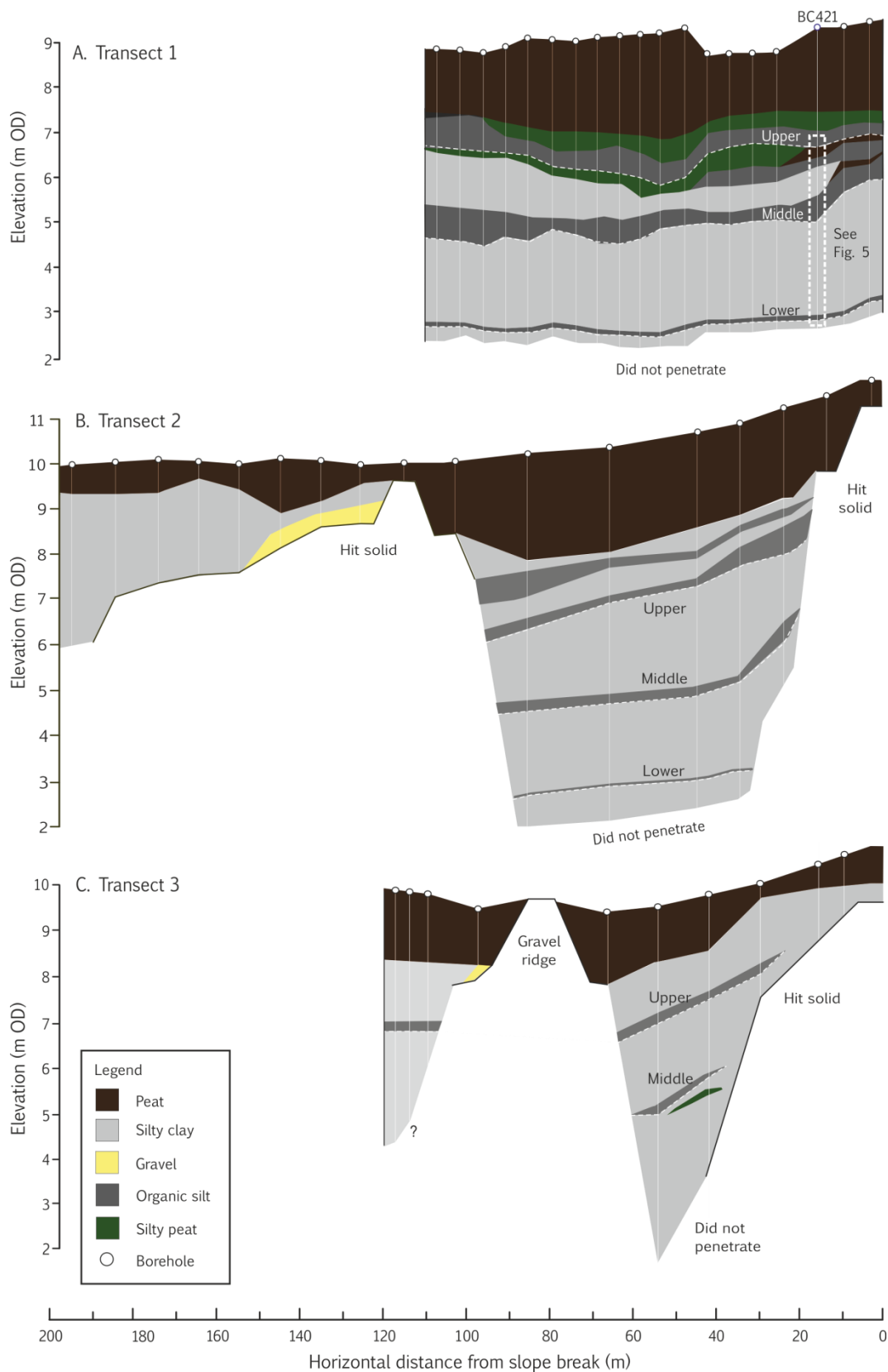


**Figure 4. Lithostratigraphy of Blair's Croft recorded along A) Transect 1, B) Transect 2 and C) Transect 3.** The reader is referred to Figures 3 and 5 for core locations and  $^{14}\text{C}$  dating of core BC421, respectively. To aid in correlations, organic beds 'lower', 'middle' and 'upper' are illustrated, but we note that our focus is on the sedimentary sequence illustrated by the stipple white outline in Transect 1 which here encompasses the lower and middle beds and their overlying minerogenic deposits.

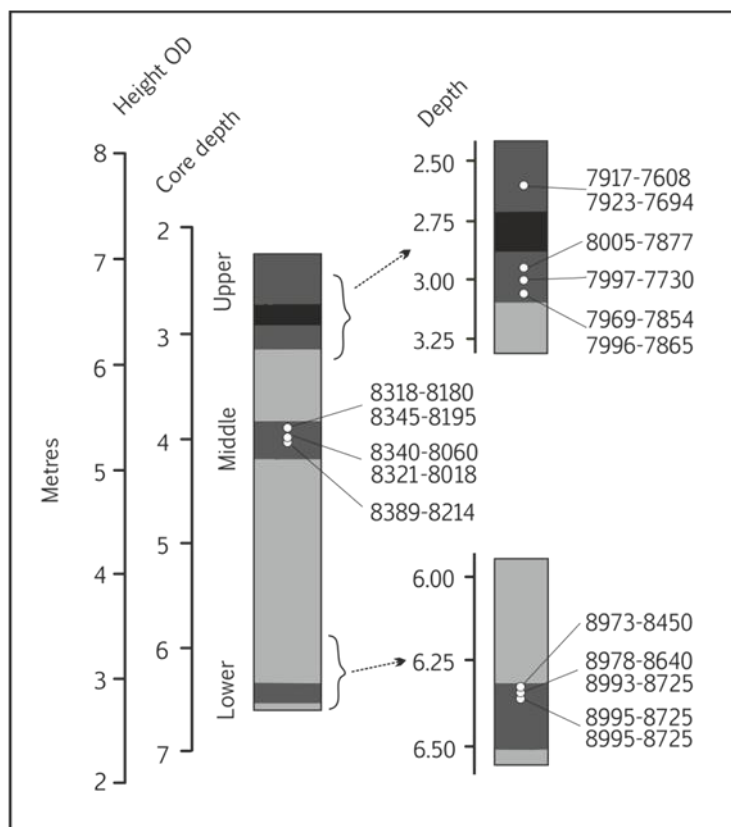
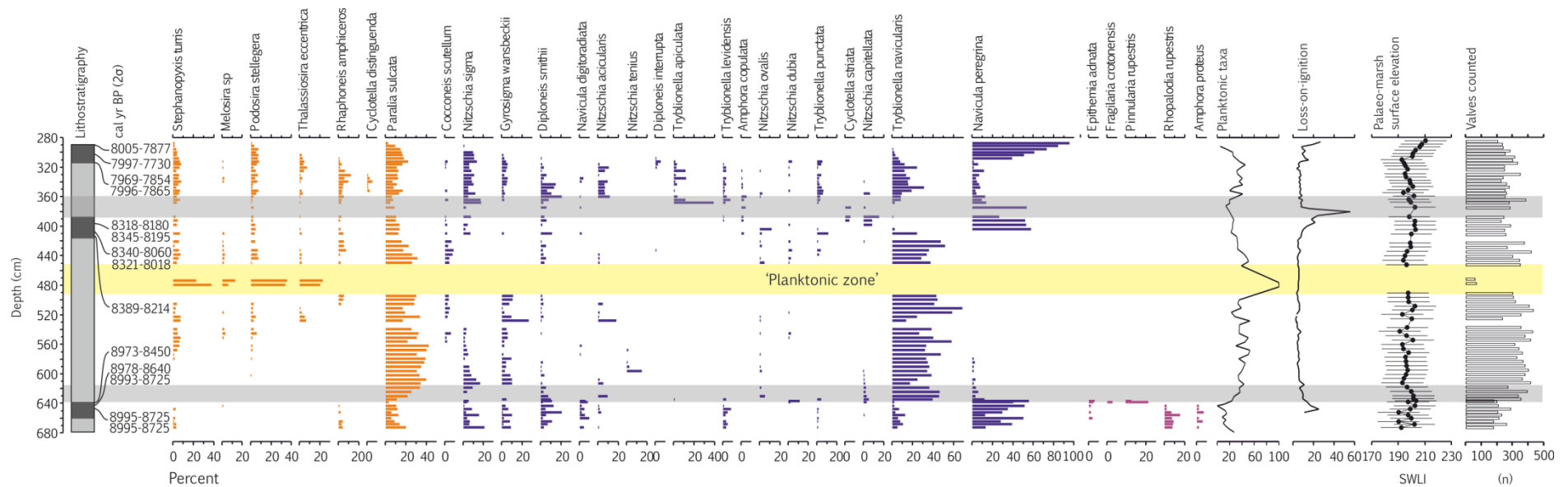
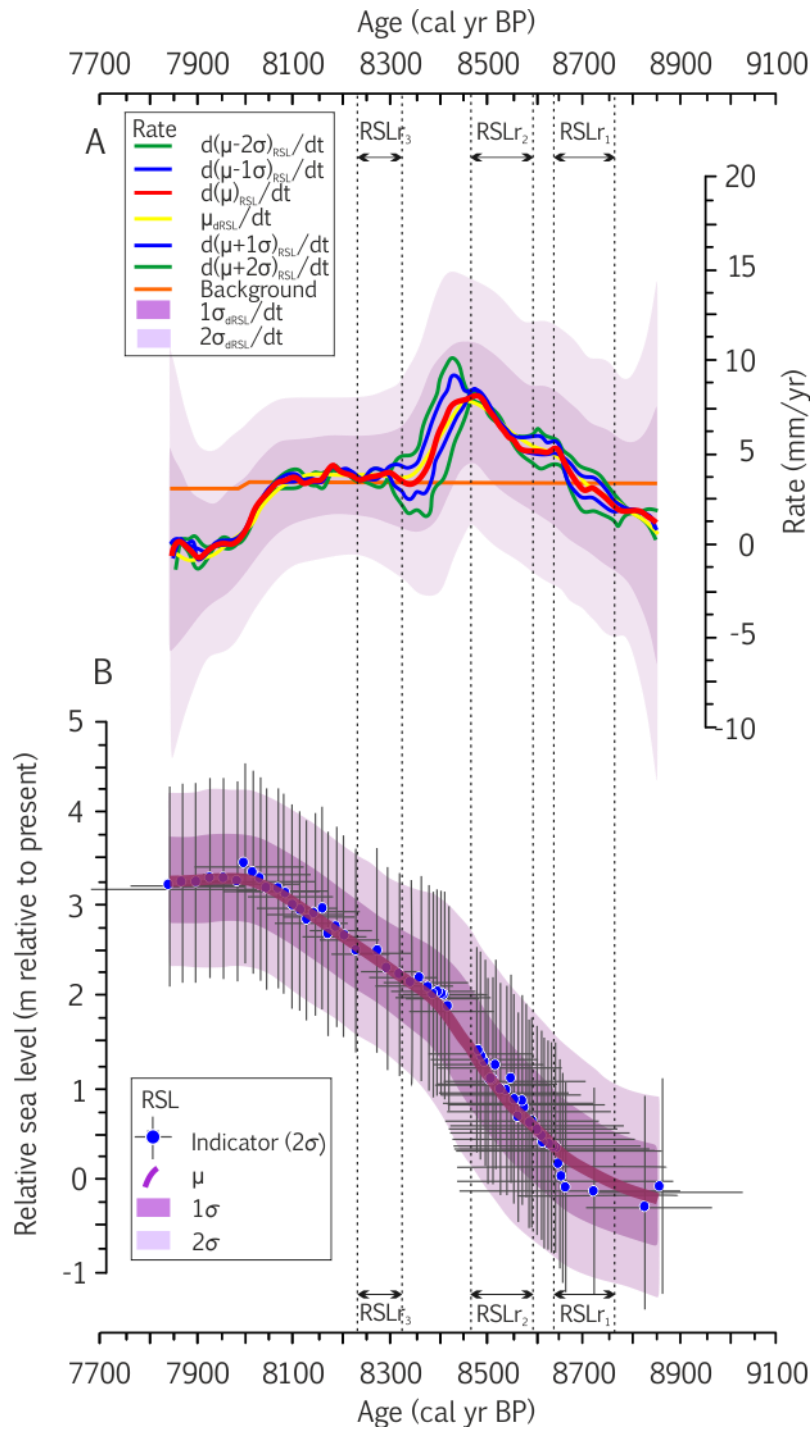


Figure 5. Radiocarbon dating of core BC421. Ages are reported as 2σ calibrated ranges (IntCal 13; Reimer et al., 2013).



**Figure 6. Diatom biostratigraphy, chronostratigraphy and LOI of core BC421.** Diatom contributions represent >5%. Palaeommarsh surface elevation (in SWLI units) is reconstructed using the component-two model (WA-PLS) of the ‘screened’ training set. For a more detailed view of sample depths of  $^{14}\text{C}$  ages, refer to Figure 5 and Table 1. Marine taxa (planktonic forms) are indicated in orange, brackish-indifferent taxa in blue and freshwater-brackish taxa in purple. Yellow shading indicates the ‘planktonic zone’. Gray shading indicates abrupt reductions in SWLI that are accompanied by stratigraphic evidence of marsh drowning (see discussion).



**Figure 9.** Relative sea-level change in the Cree Estuary for the period 8800 -7700 cal yr BP. **a.** Rates of relative sea-level change in **a.** are inferred from the relative sea-level reconstruction in **b.** The orange line depicts site-specific rates of millennial-scale RSL change as depicted by the Bradley et al. (2011) GIA model. RSL jumps (dashed lines;  $RSLr_1$ ,  $RSLr_2$ ,  $RSLr_3$ ) are determined where rates of rise exceed the background trend in three differentiated RSL curves ( $d\mu_{RSL}/dt$ ,  $d(\mu-\sigma)_{RSL}/dt$ ,  $d(\mu+\sigma)_{RSL}/dt$ ).



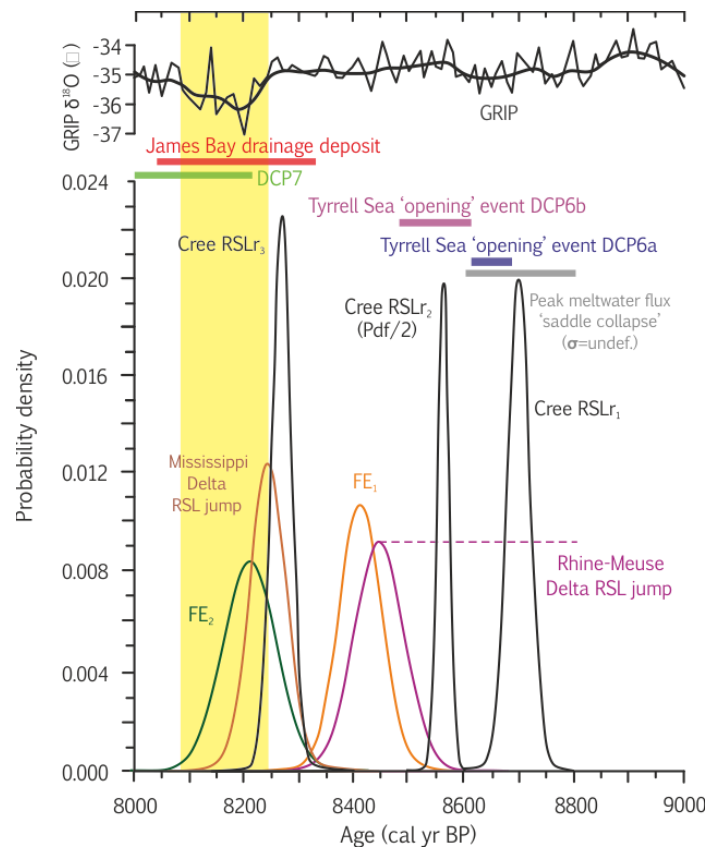


**Figure 8. Timing and sequence of climate, ocean and sea-level events in the North Atlantic between 9000 and 8000 cal yr BP.** Timing of events are expressed as age probability density functions (pdfs) ( $3\sigma$ ) and horizontal bars ( $2\sigma$  probability ranges). Probability density functions of RSL<sub>1</sub>, RSL<sub>2</sub> and RSL<sub>3</sub> (black curves) in the Cree estuary from this study are plotted alongside DCP6a (blue bar) and DCP6b (purple bar) from Jennings et al. (2015), the James Bay drainage deposit (red bar; Roy et al., 2005), the onset of sudden sea-level rise in the Rhine-Meuse Delta (purple curve; Hijma and Cohen, 2010) and Mississippi Delta (brown curve; Li et al., 2012) and the two North Atlantic surface cooling and freshening events (FE<sub>1</sub>; orange curve, FE<sub>2</sub> light blue curve) inferred from revised chronology of Kleiven et al. (2008). Peak meltwater discharge (modelled) associated with separation of the Keewatin and Labrador ice-dome ‘saddle’ (Gregoire et al., 2012) is shown as a grey bar, but note has no strict statistical definition. Yellow shading depicts the full duration of the 8.2 event as determined from Greenland ice-core records by Thomas et al. (2007).



**Table 1.** Radiocarbon dates from BC421. Samples B1(a) and B1(b) (dark gray) are excluded from the age model because they are taken from the base of the ‘upper’ organic bed and are too young to be associated with the 8.2 kyr BP event, but provide a maximum age of barrier activity at its present position. Sample B is not included because of a minor age reversal with preceding samples (light grey). AMS = accelerator mass spectrometry. \*Calibrated with the IntCal13 calibration curve (Reimer et al. 2013) in OxCal 4.2 (Bronk Ramsey, 2008). Modelled weighted means of duplicate ages are highlighted bold.

Sample Code	Identifier	Depth (cm)	Height (m OD)	Dating method	Material dated	Reported <sup>14</sup> C age ( $\pm 1\sigma$ lab error)	Calibrated* range ( $2\sigma$ )
SUERC-44407	B1(b)	259.5	6.90	Duplicate AMS	<i>Phragmites australis</i>	6890 $\pm$ 64	7917-7608
SUERC-44406	B1(a)	259.5	6.90	Duplicate AMS	<i>Phragmites australis</i>	6963 $\pm$ 36	7923-7694
SUERC-44405	B	294.5	6.55	Single AMS	<i>Phragmites australis</i>	7127 $\pm$ 26	8005-7877
SUERC-44400	C	300.5	6.49	Single AMS	<i>Phragmites australis</i>	7049 $\pm$ 65	7997-7730
SUERC-42712	D(b)	307	6.42	Duplicate AMS	<i>Phragmites australis</i>	7088 $\pm$ 26	7969-7854
SUERC-44399	D(a)	307	6.42	Duplicate AMS	<i>Phragmites australis</i>	7107 $\pm$ 26	7996-7865 <b>(7968-7871)</b>
SUERC-44371	Q(b)	389	5.60	Duplicate AMS	<i>Alnus</i>	7409 $\pm$ 26	8318-8180
SUERC-42711	Q(a)	389	5.60	Duplicate AMS	<i>Alnus</i>	7452 $\pm$ 25	8345-8195 <b>(8315-8188)</b>
SUERC-44398	R(b)	395.5	5.54	Duplicate AMS	<i>Phragmites australis</i>	7344 $\pm$ 65	8321-8018
SUERC-44397	R(a)	395.5	5.54	Duplicate AMS	<i>Phragmites australis</i>	7392 $\pm$ 39	8340-8060 <b>(8339-8201)</b>
SUERC-44386	T	402	5.47	Single AMS	<i>Phragmites australis</i>	7507 $\pm$ 25	8389-8214
SUERC-44387	U	631	3.18	Single AMS	<i>Phragmites australis</i>	7831 $\pm$ 65	8973-8450
SUERC-42709	V(b)	632	3.17	Duplicate AMS	<i>Alnus</i>	7936 $\pm$ 27	8978-8640
SUERC-44385	V(a)	632	3.17	Duplicate AMS	<i>Alnus</i>	7977 $\pm$ 26	8993-8725 <b>(8936-8650)</b>
SUERC-44369	W(b)	632	3.17	Duplicate AMS	<i>Alnus</i>	7980 $\pm$ 27	8995-8725

SUERC-42708	W(a)	633	3.16	Duplicate AMS	<i>Alnus</i>	7982 ± 27	8995-8725 <b>(8960-8660)</b>
-------------	------	-----	------	---------------	--------------	-----------	---------------------------------

	<b>Position in stratigraphy / record</b>	<b>Minimum age (cal yr BP)</b>	<b>Maximum age (cal yr BP)</b>	<b>Minimum age (yrs BP) from start of 8.2 event</b>	<b>Maximum age (yrs BP) from start of 8.2 event</b>	<b>Reference</b>
8.2 event	All	8086	8247	0	0	Thomas et al. (2007)
Cree Estuary RSLr <sub>3</sub>	Start	8218	8323	-29	237	This study
FE <sub>2</sub>	Start	8114	8308	-133	222	Kleiven et al. (2008); this study
Mississippi Delta	All	8180	8310	-67	224	Li et al. (2011)
James Bay drainage deposit	All	8032	8323	-215	237	Roy et al. (2011)
FE <sub>1</sub>	Start	8338	8492	91	406	Kleiven et al. (2008); this study
Cree Estuary RSLr <sub>2</sub>	All	8465	8595	288	509	This study
Rhine-Meuse Delta	Start	8455	8587	208	501	Hijma and Cohen (2010)
Cree Estuary RSLr <sub>1</sub>	Start	8640	8760	393	674	This study
DCP6b	Start	8489	8609	242	523	Jennings et al. (2015)
Keewatin and Labrador saddle collapse	Peak	8600	8800	353	714	Gregoire et al. (2012)
DCP6a	Start	8609	8694	362	608	Jennings et al. (2015)

**Table 2. Timing of abrupt events within the critical time interval.** Ages presented are  $2\sigma$  calibrated ranges with respect to BP (AD 1950), with the exception of the Cree RSL jumps (3 sigma of the differentiated record) and the Thomas et al. (2007) estimate of the timing of the 8.2 event (full 3 sigma uncertainty range).

**Table 3. Magnitudes of abrupt sea-level change within the critical time interval.** Local magnitude (Local) and Fingerprint-corrected value (Global) assumes a LIS source of freshwater release with fingerprint values of 20% for the Mississippi Delta and 70% for the Cree Estuary and Rhine-Meuse Delta, respectively (after the geophysical model predictions of Kendall et al. (2008)).

	Differentiated RSL curve reconstruction					RSL rate reconstruction				
	$d(\mu-2\sigma)_{RSL}/dt$	$d(\mu-\sigma)_{RSL}/dt$	$d\mu_{RSL}/dt$	$d(\mu+\sigma)_{RSL}/dt$	$d(\mu+2\sigma)_{RSL}/dt$	$(\mu-2\sigma)_{dRSL/dt}$	$(\mu-\sigma)_{dRSL/dt}$	$\mu_{dRSL/dt}$	$(\mu+\sigma)_{dRSL/dt}$	$(\mu+2\sigma)_{dRSL/dt}$
<b>RSLR<sub>3</sub></b>										
<b>Local</b>	0.37	0.39	0.40	0.41	0.43	-0.10	0.15	0.40	0.65	0.90
<b>Global</b>	0.54	0.55	0.57	0.59	0.61	-0.15	0.21	0.57	0.93	1.29
<b>RSLR<sub>2</sub></b>										
<b>Local</b>	0.67	0.69	0.70	0.72	0.73	-0.05	0.27	0.66	1.05	1.44
<b>Global</b>	0.96	0.98	1.00	1.02	1.04	-0.07	0.39	0.95	1.50	2.06
<b>RSLR<sub>1</sub></b>										
<b>Local</b>	0.24	0.30	0.35	0.40	0.45	-0.42	-0.03	0.36	0.75	1.15
<b>Global</b>	0.35	0.42	0.50	0.57	0.65	-0.60	-0.04	0.52	1.08	1.64
<b>Sum total of RSLR<sub>1</sub> and RSLR<sub>2</sub>:</b>										
<b>Local</b>	1.34	1.40	1.45	1.50	1.56	-0.58	0.39	1.42	2.46	3.49
<b>Global</b>	1.92	2.00	2.07	2.15	2.23	-0.82	0.56	2.03	3.51	4.99